Cell Reports

Resource

Cell-Type- and Brain-Region-Resolved Mouse Brain Lipidome

Graphical Abstract

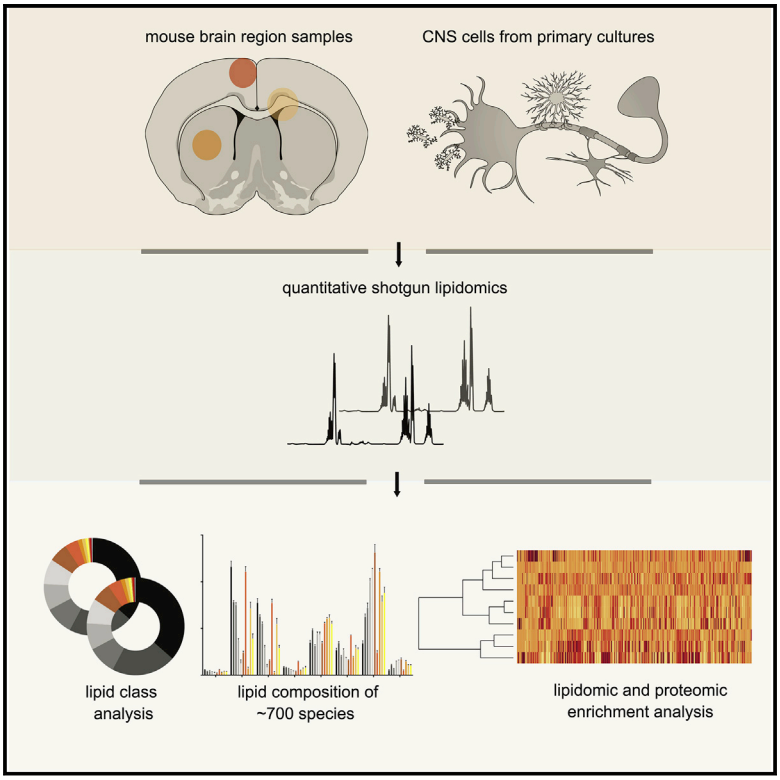

Authors

Dirk Fitzner, Jakob M. Bader, Horst Penkert, ..., Matthias Mann, Christian Klose, Mikael Simons

Correspondence

d.fitzner@med.uni-goettingen.de (D.F.), msimons@gwdg.de (M.S.)

In Brief

Fitzner et al. perform extensive lipidome analyses on the mouse brain and its major cell types and integrate lipid with protein expression profiles to predict lipid pathways enriched in specific cells and brain regions. The study serves as a resource for better understanding of brain development and function.

Highlights

- Brain-region- and cell-type-resolved lipidomic profiling
- Definition of differences in lipid profiles of CNS cell types
- Integration of lipid with protein expression profiles predicts lipid pathways
- Aging alters brain lipid profiles with regional differences

Fitzner et al., 2020, Cell Reports *32*, 108132
September 15, 2020
https://doi.org/10.1016/j.celrep.2020.108132

CellPress

Cell Reports

CellPress
OPEN ACCESS

Resource

Cell-Type- and Brain-Region-Resolved Mouse Brain Lipidome

Dirk Fitzner,[1,2,11,*] Jakob M. Bader,[4] Horst Penkert,[3,6,8,9] Caroline G. Bergner,[2,5] Minhui Su,[3,6] Marie-Theres Weil,[1] Michal A. Surma,[7] Matthias Mann,[4,10] Christian Klose,[7] and Mikael Simons[1,3,6,8,11,12,*]

[1]Max Planck Institute of Experimental Medicine, 37075 Göttingen, Germany
[2]Department of Neurology, University of Göttingen Medical Center, 37075 Göttingen, Germany
[3]Institute of Neuronal Cell Biology, Technical University Munich, 80802 Munich, Germany
[4]Department of Proteomics and Signal Transduction, Max Planck Institute of Biochemistry, 82152 Martinsried, Germany
[5]Department of Neuropathology, University of Göttingen Medical Center, 37075 Göttingen, Germany
[6]German Center for Neurodegenerative Diseases (DZNE), 81377 Munich, Germany
[7]Lipotype, 01307 Dresden, Germany
[8]Munich Cluster of Systems Neurology (SyNergy), 81377 Munich, Germany
[9]Department of Neurology, School of Medicine, Technical University of Munich (TUM), 81675 Munich, Germany
[10]Clinical Proteomics Group, Proteomics Program, Novo Nordisk Foundation Center for Protein Research, University of Copenhagen, Copenhagen, Denmark
[11]Senior author
[12]Lead Contact
*Correspondence: d.fitzner@med.uni-goettingen.de (D.F.), msimons@gwdg.de (M.S.)
https://doi.org/10.1016/j.celrep.2020.108132

SUMMARY

Gene and protein expression data provide useful resources for understanding brain function, but little is known about the lipid composition of the brain. Here, we perform quantitative shotgun lipidomics, which enables a cell-type-resolved assessment of the mouse brain lipid composition. We quantify around 700 lipid species and evaluate lipid features including fatty acyl chain length, hydroxylation, and number of acyl chain double bonds, thereby identifying cell-type- and brain-region-specific lipid profiles in adult mice, as well as in aged mice, in apolipoprotein-E-deficient mice, in a model of Alzheimer's disease, and in mice fed different diets. We also integrate lipid with protein expression profiles to predict lipid pathways enriched in specific cell types, such as fatty acid β-oxidation in astrocytes and sphingolipid metabolism in microglia. This resource complements existing brain atlases of gene and protein expression and may be useful for understanding the role of lipids in brain function.

INTRODUCTION

Transcriptome and proteome analyses of CNS cell populations have generated large collections of mRNA and protein expression resources across different brain regions and cell types (Davie et al., 2018; Mahfouz et al., 2017; Sharma et al., 2015; Zhang et al., 2014; Hawrylycz et al., 2012; Heiman et al., 2008). However, a related effort to resolve the brain lipidome is missing. Among the body organs, the brain is, after adipose tissue, the second-most lipid-rich organ (Dawson, 2015) with important functions of lipids in the formation of membranes, intracellular signaling, and energy production (Aureli et al., 2015; Harayama and Riezman, 2018; Ingólfsson et al., 2017). Because of the convoluted structure of neuronal and glial membranes with their vastly arborized and differentially shaped processes, membrane lipids have important structural roles in the CNS (Chrast et al., 2011; Lauwers et al., 2016, 2016; Schmitt et al., 2015). The astonishing morphological complexity of the cells within the CNS comprises neurons and glia, among them oligodendrocytes, astrocytes, and microglia. Oligodendrocytes are primarily engaged in membrane synthesis, because their major function is to generate myelin, a multilamellar membrane stack that is required to insulate axons and to allow rapid nerve propagation (Stadelmann et al., 2019). In contrast, astrocytes regulate the extracellular ion balance, recycle neurotransmitters, shape synaptic circuits, and maintain the blood-brain barrier (Khakh and Deneen, 2019; Santello et al., 2019), whereas microglia functions are mainly related to immune response and maintaining brain homeostasis (Butovsky and Weiner, 2018; Deczkowska et al., 2018). Not only is the brain tissue highly enriched in lipids, but its complex function and morphology is also reflected by an astonishing variety of lipid species. About 75% of lipids of mammals are exclusive to neural tissues, demonstrating the unique requirements of specific lipids for brain function. Although the brain lipidome appears to be generally conserved among species, the increasing functional complexity in evolution is reflected by a larger variety and increased tissue specificity of the brain lipid species composition (Bozek et al., 2015).

Detailed lipid profiles of CNS cells or brain regions is sparse, but the available information indicates that certain lipid classes

and even lipid species appear to be enriched in distinct cell types or brain areas. For example, neurons and myelin contain high levels of cholesterol (Chol) (Camargo et al., 2017; Ingólfsson et al., 2017; Saher et al., 2005), whereas galactosylceramides are typically accumulating exclusively in the oligodendroglial membrane during myelination (Schmitt et al., 2015). However, until recently, because of technical difficulties, robust, reproducible quantification of entire lipid profiles in multiple samples has been difficult obtain. This situation has changed with the development of comprehensive, high-throughput, and quantitative shotgun lipidomics (Gross, 2017; Wang et al., 2016; Surma et al., 2015). Taking advantage of this technology, we provide a quantitative cell-type-resolved assessment of the mouse brain lipidome that highlights the cell-type-specific lipids. We quantified around 700 lipid species and evaluated lipid features such as fatty acyl chain length, hydroxylation, and number of acyl chain double bonds (DBs) to obtain a detailed cell-type- and brain-region-resolved profile of CNS lipid composition. We correlated the lipidomic dataset obtained with proteomic data. In addition, we evaluated the influence of dietary fatty acids on the brain lipidome, and we performed a region-resolved lipidomic analysis of the mouse brain during aging and under pathological conditions. This database represents a new resource for the neuroscience community that complements existing mRNA and proteome studies.

RESULTS

Cell-Type- and Brain-Region-Resolved Adult Brain Lipidome and Coverage

To resolve the cell-type- and location-specific lipidome of the CNS, we carried out in-depth lipid analysis of various CNS-derived primary cell cultures and tissue samples of distinct brain regions. Transcriptomic analysis of single-cell types can be performed by collecting material through laser microdissection, fluorescence-activated cell sorting (FACS), or immunopanning of labeled cells from tissue (Hawrylycz et al., 2012; Skinnider et al., 2019; Ximerakis et al., 2019). However, these procedures lead to loss of the highly branched and complex cellular membranes and are therefore not an option for lipidome analysis. In addition, most cells in the CNS are tightly connected to one another, which rules out cell-specific membrane separations from the intact brain (Tietz and Engelhardt, 2015). Thus, we prepared primary cultures of the major CNS cell types to evaluate cell-type-specific membrane compositions (Sharma et al., 2015). Cell pellets were also prepared from neurons and oligodendrocytes at different stages of development (1, 2.5, and 4 days *in vitro* for oligodendrocytes and 5, 10, and 16 days *in vitro* for cortical neurons) to include a developmental analysis of the cellular lipid composition.

To resolve the lipidome of distinct regions of the adult mouse, brain samples from specific anatomical structures were collected by microdissection from 9-week-old male mice in triplicate using a rodent brain matrix 1-mm coronal slicer according to coordinates obtained from the Mouse Brain Library. These regions included the brain stem, corpus callosum, cerebellum, hippocampus, motor cortex, olfactory bulb, optic nerve, prefrontal cortex, striatum, and thalamus. All animals were fed a standard diet. Cell pellets or tissue punches were subjected to two-step lipid extraction and shotgun lipidomics (Ejsing et al., 2009; Sampaio et al., 2011). Lipidomic data were normalized to internal standards, enabling us to determine the absolute quantity of more than 700 unique lipid species of 24 analyzed lipid classes in picomol. The complete lipidomic dataset is presented in Table S1. Data were transformed to percentage of moles per sample for each lipid, allowing direct comparison of samples with different total lipid amounts. In addition, multivariate statistical data analysis was applied to evaluate the variations in the cellular lipidomes. The average quantity of the 13 most abundant lipid classes is shown in Figure 1 for samples obtained from either primary cell cultures (Figure 1A) or mouse brain tissue (Figure 1B). A principal-component analysis (PCA) was used to visualize variation and to highlight robust patterns in the datasets in a two-dimensional score plot (Figures 1C and 1D). The biological replicates clearly clustered together, demonstrating excellent technical and biological reproducibility. When comparing the different cell types, we found that oligodendrocytes were the most diverging cell type, most likely because of their role in producing myelin, with its unique lipid composition (Figure 1C). PCA of brain regions also showed clustering of replicates, whereas samples were segregated in both dimensions, indicating differences in the lipid composition. Samples from the optic nerve, brain stem, and prefrontal cortex were separated particularly from other brain regions, suggesting marked differences in the lipid composition of these areas (Figure 1D).

From the 23 lipid classes of the cell-originating lipidome and the 24 classes of the tissue-originating lipidome, we selected 13 lipids that compromised more than 99% of the absolute molar lipid mass for further analysis. The prevalence of these lipids in the two datasets is shown in Figure 1A for the cell lipidome and in Figure 1B the tissue lipidome. The quantity of the major lipid classes is depicted in relation to either the cellular origin (Figure 1E) or distinct brain regions (Figure 1F).

Overall, phosphatidylcholine (PC), Chol, and phosphatidylethanolamine (PE) are the three most common classes in both sets of samples. However, a range of lipid-class profiles and patterns can be observed when comparing lipid composition of the cellular populations and distinct brain regions.

Definition of Differences in Lipid Classes of CNS Cell Types

Next, we examined possible enrichments of lipid classes in cultured CNS-derived mature cell types. Figure 2A illustrates the composition of the 20 most abundant lipid classes in the four CNS-derived cell types as parts of the overall lipid content. A heatmap representation of lipid-class composition displays the diversity of the lipidomes in oligodendrocytes, microglia, astrocytes, and neurons (Figure 2B). We determined the quantity of each lipid class as the percentage of the total lipid amount for each sample (Figure 2C). We confirmed that sulfatide (Sulf) and hexosylceramide (HexCer), two structural lipids of myelin membrane, are enriched in mature oligodendrocytes. Elevated levels of PC, PE, Chol, and ceramide (Cer) were observed in cultured neurons. Astrocytes were enriched in phosphatidylserine (PS), phosphatidylinositol (PI), and diacylglycerol (DAG). Interestingly, we observed that microglia displayed high molar concentrations of sphingomyelin (SM) and phosphatidylglycerol (PG). We were

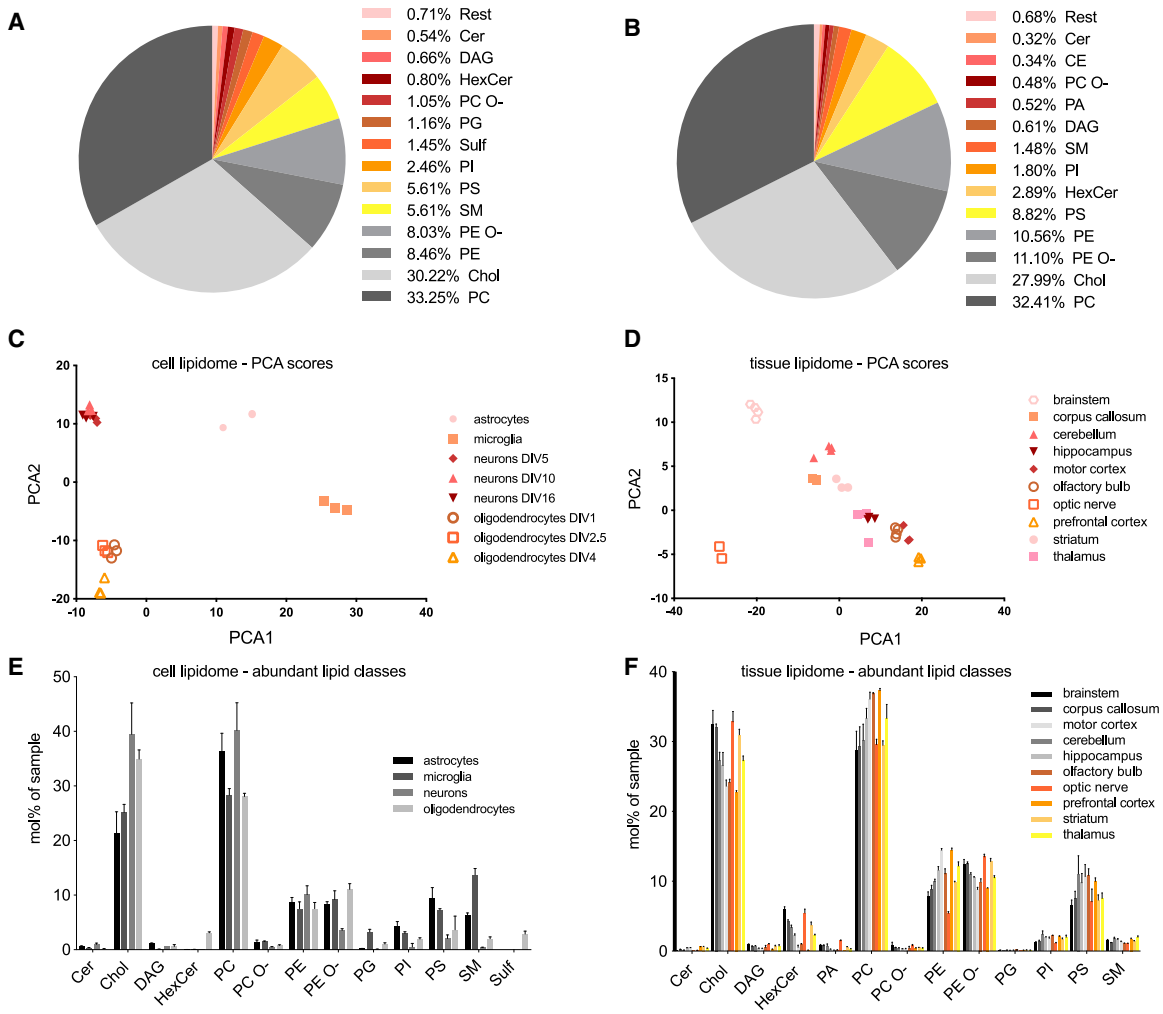

Figure 1. Lipid-Class Distribution in Mouse CNS Cells and Tissue

(A and B) Average distribution of the 13 most abundant lipid classes (A) in primary CNS cell cultures and (B) in CNS brain regions, displayed as parts of the whole.

(C and D) PCA of the lipidome of (C) cultured CNS cell types after various days *in vitro* (DIV) or (D) 10 mouse brain regions. One datapoint of the optic nerve was excluded as an outlier because of technical problems. Lipid species' percentage of moles per cell type or region were used as input data.

(E and F) Lipid composition in percentage of moles per sample representing the 13 most abundant lipid classes of (E) mature cultured CNS cells or (F) mouse brain regions. Mean values and standard deviation for each cell type or brain region (n = 3 for cell types and regions, except n = 4 for brain stem, cerebellum, and olfactory bulb).

Rest, remaining unspecified lipid classes. Abbreviations of lipid classes are defined by Lipid Maps classification (Table S2). See also Table S1.

also able to show how the lipid composition of oligodendrocytes and neurons changed during development *in vitro* (Figures S1A and S1B). We analyzed three time points of cellular differentiation in both cell types. Among the major lipid classes, Chol showed the most profound changes in neurons, with the amount increasing over time. In addition, lysophospholipids such as lysophosphatidylchline (LPC) increased during neuronal differentiation (Figure S1A). Oligodendrocytes displayed a steady increase of lipids enriched in myelin, such as Chol, HexCer, ether-linked phosphatidylethanolamine (PE O-), and Sulf, at the expense of PC, which decreased during oligodendrocyte maturation (Figure S1B).

Because each cell type is composed of unique lipid compositions, we wondered whether differences in lipid metabolic pathways are also detectable on the proteome level. We have previously performed an in-depth analysis of primary cultured cells to obtain a complete proteome inventory of major CNS cell types (Sharma et al., 2015). We used these data for clustering and cluster-specific enrichment analysis of lipid-related metabolic pathways using Gene Ontology biological processes (GOBPs), Gene Ontology cellular components (GOCCs), Gene Ontology molecular function (GOMF), Kyoto Encyclopedia of Genes and Genomes (KEGG), PathBank, and Uniprot protein families. We assessed the enrichment of the pathways and components by unsupervised hierarchical clustering and found that most proteins could be divided into five distinct clusters (Figures 3A–3C; Table S3). Lipid-related pathways and biological functions enriched in microglia include lipid degradation,

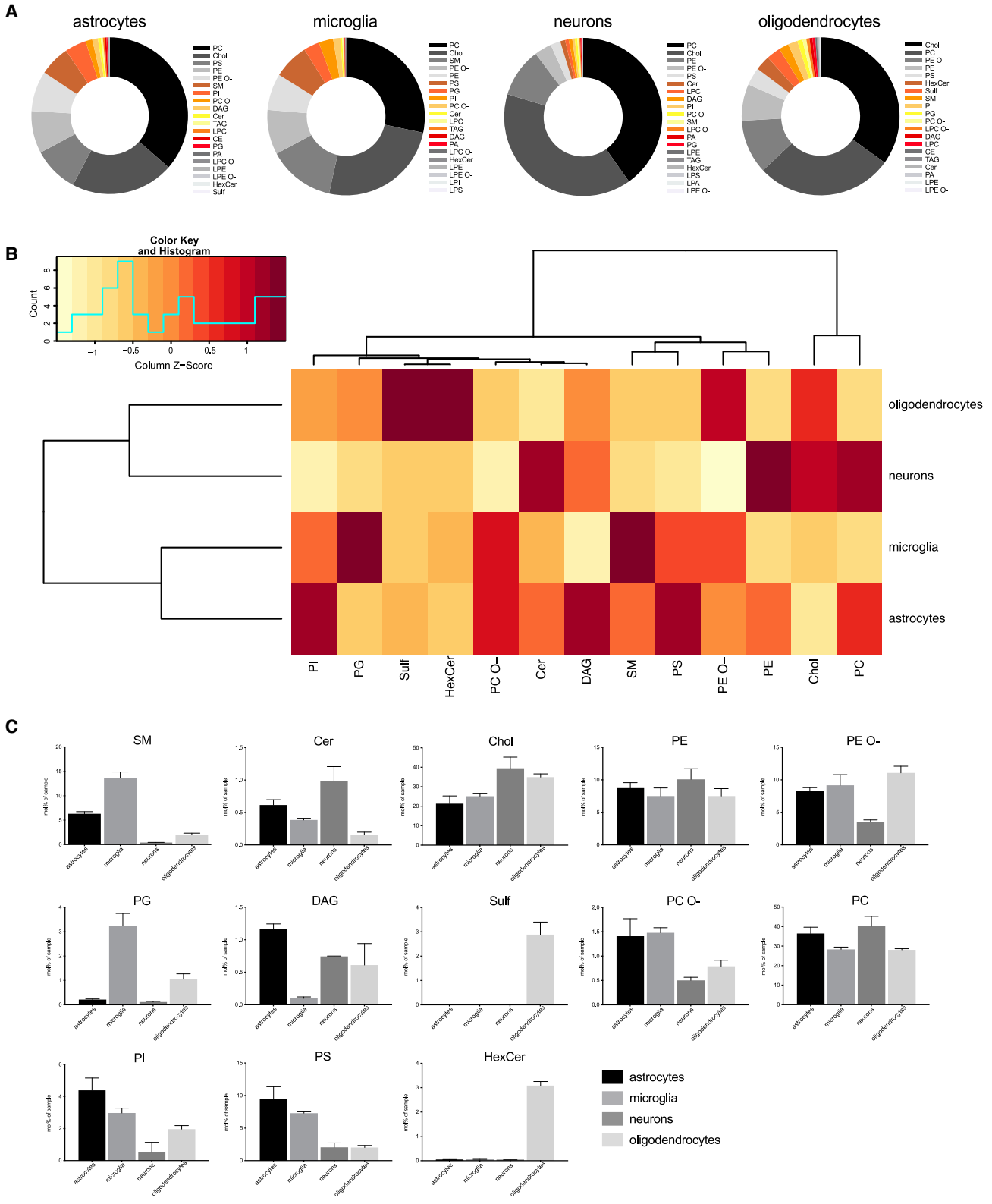

(legend on next page)

prostaglandin, arachidonic, and sphingolipid (SP) pathways (Figure 3D). For oligodendrocytes, we found the expected pathways involving lipid and Chol biosynthesis. For example, we observed higher *Z* scores of biosynthetic pathways involved in the synthesis of galactosylceramide, a member of the lipid class HexCer, which was particularly enriched in the oligodendrocytic lipidome (Figure 3G). We were able to correlate the decrease in concentration of PC during oligodendrocyte development in the lipidome data with the increase of protein expression in pathways regulating PC catabolism (Figure 3E). Pathways enriched in neurons involve DAG kinase, glycerophospholipid (GPL), and glycosylphosphatidylinositol (GPI)-anchor biosynthesis, and those enriched in astrocytes involve mitochondrial β-oxidation of medium- and long-chain saturated fatty acids and fatty acid β-oxidation. Because our lipid analysis revealed that microglia are enriched in SPs, we performed clustering of SP-related pathways, which confirmed that many biological processes associated with SP metabolism, including regulation of SP biosynthesis, sphinganine-1-phosphate biosynthesis, SP translocation, and catabolism, are enriched in microglia (Figure 3H). Clustering of steroid-related pathways showed that distinct metabolic processes are divided among the different cell types. Although pathways associated with sterol biosynthesis are overrepresented in neurons and oligodendrocytes (Figure 3F), sterol storage and efflux pathway are assigned to microglia (Figure 3F).

Definition of Differences in Lipid Classes within Different Brain Regions

Because regional specialization is a hallmark of the structure and function of the CNS, we determined whether specific lipid classes are detected within the different major regions, including the brain stem, corpus callosum, cerebellum, hippocampus, motor cortex, olfactory bulb, optic nerve, prefrontal cortex, striatum, and thalamus. As judged by the PCA, the optic nerve, brain stem, and prefrontal cortex were brain regions with the most distinct lipid composition, whereas the remaining seven regions clustered more tightly (Figure 1D). The hierarchical clustering shows that brain regions containing more myelin, such as the optic nerve, brain stem, striatum, and corpus callosum, group together (Figure 4A). Clustering and analysis of the mole percentage values of the 13 most abundant lipid classes identify HexCer, Chol, and PE O- as the most enriched lipids in these 4 brain regions (Figure 4B). In contrast, brain regions such as the prefrontal cortex or the motor cortex that are depleted in myelin and enriched in neuronal cell bodies and dendrites have a diametrically opposed lipid composition, with a higher proportion of PC, PS, PE, PI, SM, Cer, and PG. This correlation is shown in Figure 4C by plotting the relative differences in percentage of moles from the average of the lipid-class distribution in the prefrontal cortex compared with the optic nerve. We also calculated the difference from the average percentage of moles of abundant lipid classes presented in Figure S1C, again demonstrating the considerable difference of regional tissue lipid composition among different brain regions.

Next, we analyzed lipid metabolic pathways in these brain regions on the proteome level. We used brain-region-resolved proteome data for clustering and cluster-specific enrichment analysis of lipid-related metabolic pathways and found that most proteins could be divided into five distinct clusters (Figures S2A–S2D; Table S4). Consistent with its high myelin content, proteins related to galactosylceramide biosynthetic processes were enriched in the optic nerve, whereas galactosylceramide catabolic processes were highest in the brain stem (Figure S2G). In addition, the optic nerve was enriched in processes related to Chol biosynthesis (Figures S2D and S2F), whereas proteins associated with Chol storage were highest in the cerebellum (Figure S2F). When analyzing terms such as protein lipidation, DAG kinase signaling, ATG8 family, and GPI-anchor, region-specific differences were detected (Figure S3). Interestingly, the brain stem appeared to be de-enriched for most lipid-related metabolic pathways, with the exception of the autophagy-related ATG8 family of proteins (Figure S3B).

Analysis of Lipid Species in Cell Types and Brain Regions

Because our dataset includes not only the quantities of 24 lipid classes but also the absolute quantities of 748 individual lipid species belonging to these classes, we analyzed the distribution and enrichment of the species according to cell type or brain region by hierarchical clustering of lipid species (Figure S4). To identify species with cellular or regional enrichment, we screened and selected species with a more than 5-fold change of molar concentration and a p value of below 0.05 in both datasets (Tables S5 and S6). Among these lipid species, we found lipids that were elevated more than 20-fold in certain cell types or brain regions. Examples of such species are the enrichment of Sulf 36:1;2 or HexCer 36:1;2 in mature oligodendrocytes. Astrocytes are particularly enriched in certain PE species, namely, PE 16:0;0_18:0;0 and PE 16:0;0_16:0;0. Microglial cells are characterized by higher levels of SM species, such as SM 34:1;2 and SM 42:2;2, which are almost absent from neurons and oligodendrocytes. In addition, relative enrichment of certain PG species, such as PG 18:1;0_18:1;0 and PG 18:1;0_20:3;0, is detected in neurons (Figure 5A; Table S5).

The lipid species composition of different anatomical brain regions as shown in the heatmap (Figure S4B) is highly complex, possibly because CNS tissue hosts various cell types. Of 748 quantified species, we detected 30 species with more than 5-fold change ($p < 0.05$) and a minimal quantity of 0.5 mol %

Figure 2. Lipid-Class Composition of CNS Cell Types in Primary Cell Cultures

(A) Average distribution of the 20 most abundant lipid classes in primary CNS cell cultures (with cell types labeled above each pie chart), displayed as parts of the whole.

(B) Heatmap representing color-coded *Z* scores of lipid-class distribution of the 13 most abundant lipid classes of mature cultured CNS cells.

(C) Differences of concentration of individual lipid classes in mature CNS cell types. Data are in percentage of moles with mean and standard deviation (n = 3). Lipid class is indicated above each graph.

Lipid classes are defined by Lipid Maps classification (Table S2). See also Figure S1 and Table S1.

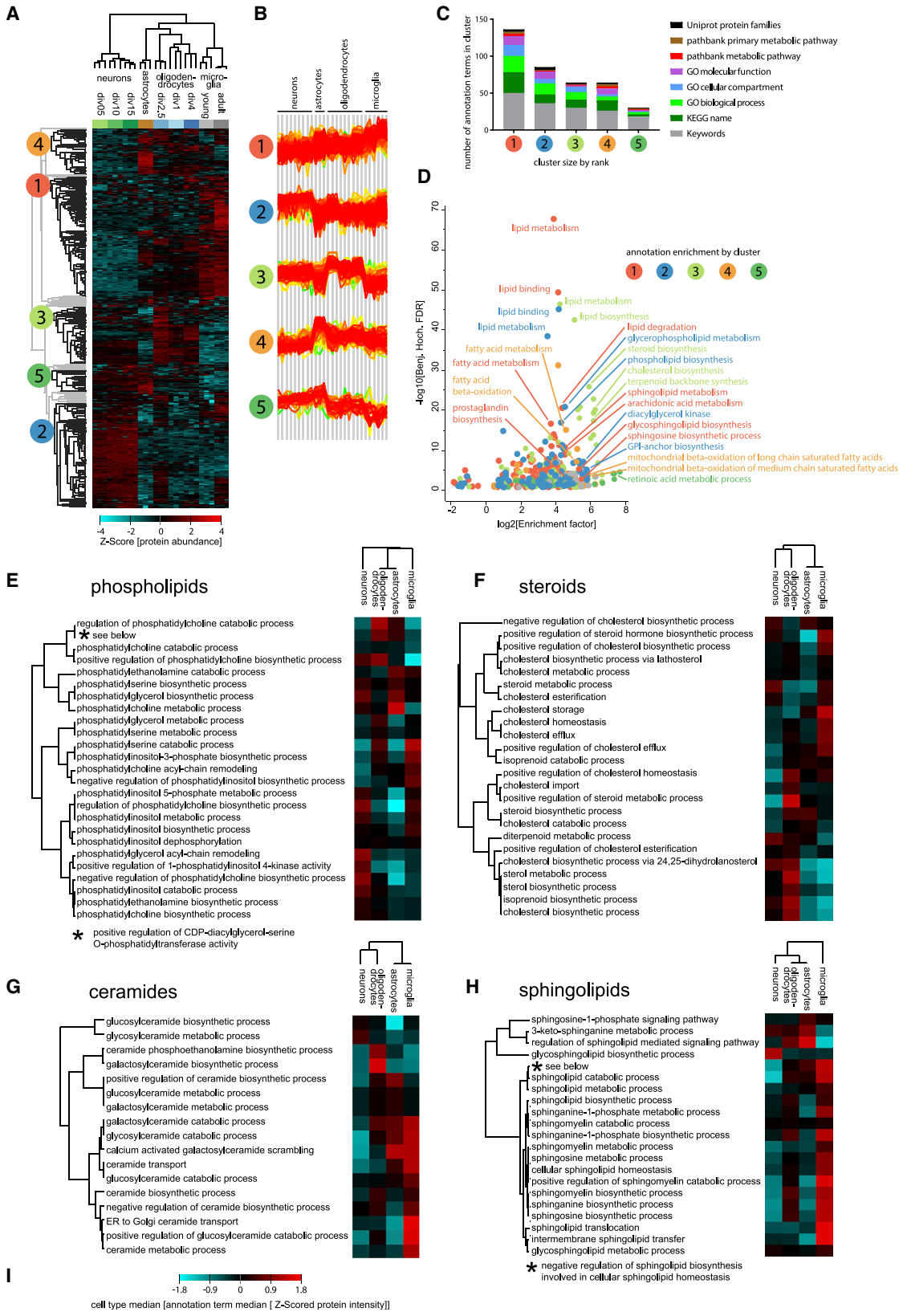

(legend on next page)

when comparing the distinct brain regions (Table S6). The quantities of some of these highly enriched species are presented in Figure 5B and comprise distinct species of HexCer and PE O- predominantly in connecting and myelin-rich brain areas such as the optic nerve or the brain stem. In contrast, cortical areas display larger differences in Cer species, such as Cer 36:2;2 or Cer 36:1;2.

Analysis of Differences in DBs, Chain Lengths, and OH Substitutions in Lipids

The applied shotgun lipidomics by measuring lipids at the level of individual molecules allows for absolute quantification of specific lipid features, such as the number of DBs, hydroxy (OH) substitutions, and acyl chain length. Chain-length distribution of GPLs varied among the cell types (Figures S5A and S7B). To evaluate the general variability of fatty acid acyl chain properties, we determined weighted averages of the number of DBs and OH substitutions, as well as the length of acyl chains of lipid subspecies in the cell-type- and tissue-based lipidomes. The weighted average values for these features were normalized by the prevalence of a certain feature, as measured by the molar fraction of relevant lipid species. We were able to observe significant differences in the length of acyl chains in GPLs and SPs with apparently reduced chain length of fatty acids in neurons (Figure 5C). We also found a reduced number of DBs in GPLs and SPs of neuronal cells, whereas the number of OH substitutes in SPs of oligodendrocytes is higher (Figure 5C; Figure S7A). Neurons and astrocytes have higher levels of PC compared with microglia and oligodendrocytes, and this enrichment is mainly represented by higher levels of PC with a shorter chain length containing, for example, a total number of 32 or 34 C atoms in both acyl chains (Figure S5A). Cellular PE levels in astrocytes (8.7 mol %) and neurons (10 mol %) are similar, but the distribution of chain length in neurons is shifted toward shorter species (Figure S5A). PS can be found in neurons at relatively low levels (2.1 mol %) compared with astrocytes (9.4 mol %) and microglia (7.3 mol %), in which PS species span a range from 32 to 40 C atoms. However, PS in neurons is almost entirely (1.86 mol %) represented by species with long chains of 40 C atoms in total (Figure S5A). The analyses of DBs revealed a relatively high proportion of saturated PE species in neurons (Figure S6A). However, PS species, which are found at lower quantities in neurons and oligodendrocytes, are mainly detectable with saturated acyl chains in oligodendrocytes including only 1 DB, whereas neuronal PS species contain unsaturated acyl chains with 4, 5, or 6 DBs (Figure S6A).

The evaluation of fatty acid features in different brain regions also demonstrated significant differences of the weighted averages of chain length, as well as the number of DBs and OH substitutes. In general, brain regions with a presumably higher content of myelinated axons such as the optic nerve, brain stem, and corpus callosum presented with shorter acyl chains in GPL and longer acyl chains in SP (Figure 5D; Figure S7D). PS was detected mainly with acyl chains of 36 or 40 C atoms. Cortical regions like the prefrontal cortex or the motor cortex contained more PS with 40 C atoms, whereas the optic nerve or the brain stem presented with higher levels of PS with 36 C atoms (Figure S5B). The same is true for PE chain length in cortical regions, where PE enrichment is represented by species with a longer acyl chain length (Figure S5B). We also found higher numbers of DBs and OH groups in SP, whereas the number of DBs in GPL fatty acids is lower in these brain regions compared with cortical regions, such as the prefrontal or motor cortex (Figure 5D; Figure S7C). For example, PE O- species with 2 or 3 DBs are present in the brain stem and optic nerve, whereas species with lower levels of saturation are found in the motor cortex, olfactory bulb, or prefrontal cortex. Consistent with a higher degree of saturation of PS species in oligodendrocytes, regions with higher myelin content, such as the brain stem, corpus callosum, or optic nerve, showed very low levels of unsaturated PS lipids, whereas most cortical areas had high levels of unsaturated PS molecules with 6 DBs (Figure S7C). The distribution of OH substitutions in GPL showed only minor variations in both cells and brain regions (data not shown).

Effects of Diets on the Adult Brain Lipidome

Next, we performed perturbation experiments to determine to what extent the mouse brain lipidome is modifiable. To determine the effect of dietary lipids on the brain lipidome, we fed adult 9-week-old mice a diet containing 5% beef tallow, 5% safflower, or 5% fish oil. Because the blood-brain barrier is still immature in the early developing brain, we also fed pregnant female mice with the different diets from the time point of conception until weaning. Offspring were kept on the diets from the time of weaning until 8 weeks of age. While maintaining the same amount of total lipids (6%–7% of wet weight), these diets varied in their composition of saturated fatty acids (43% of total fatty acids in beef tallow, 13% in safflower oil, and 29% in fish oil), polyunsaturated fatty acids (21% in beef tallow, 68% in safflower oil, and 45% in fish oil), omega-3 (n-3) fatty acids (2% in beef tallow, 2% in safflower oil, and 20% in fish oil), and omega-6 (n-6) fatty acids (18% in beef tallow, 66% in safflower oil, and 23% in fish oil). In western diets, the intake of n-6 fatty acids has increased while that of n-3 fatty acids has decreased, resulting in a large increase in the n-6/n-3 ratio from 1:1 during evolution to more than 20:1 today

Figure 3. Brain Cell Types Have Distinct Lipid-Related Proteomes

(A) Unbiased hierarchical cluster demonstrates that brain cell types have distinct expression profiles of lipid-related proteins and that developmental stage can influence lipid-related proteome expression.

(B) Profile plot shows the *Z* score abundance of proteins in the five biggest clusters identified in (A) across cell types. Profile color reflects density of profiles.

(C) Overview of annotation terms by term category enriched in protein clusters identified in (A).

(D) Enrichment factors and statistical significance of enrichment of annotation terms. Selected outlier annotations are labeled.

(E–H) Abundance profile of (E) phospholipid-related, (F) steroid-related, (G) ceramide-related, and (H) sphingolipid-related proteins on annotation-term level across brain cell types. Annotation terms are GOBP terms.

(I) Color code for heatmaps in (E)–(H).

See also Table S3.

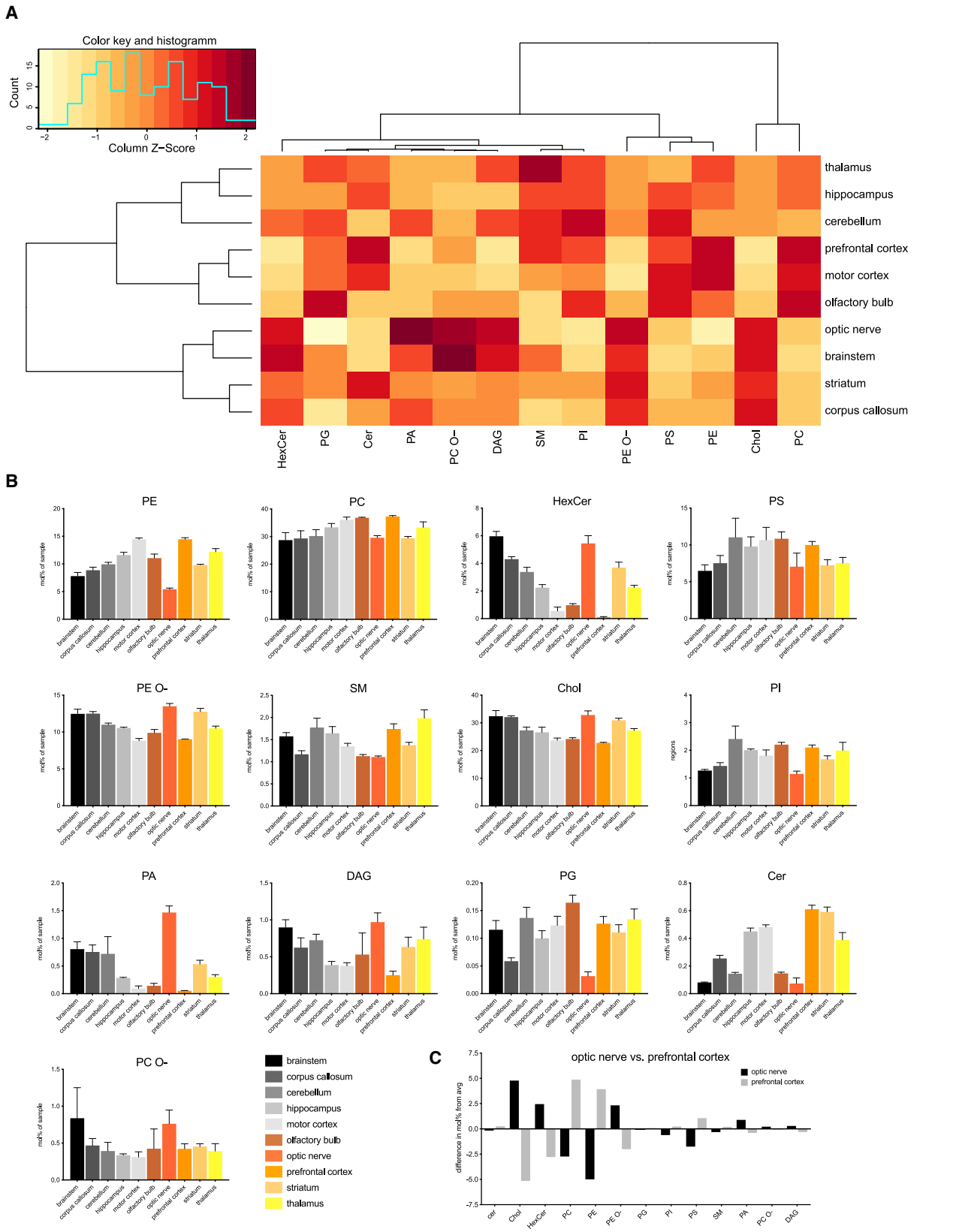

(legend on next page)

(Simopoulos, 2008). The diet containing 5% fish oil used here is with a ratio of 1:1, whereas 5% beef tallow and 5% safflower oil display ratios of 10:1 and 44:1 of n-6/n-3 fatty acids, respectively. At the end of the feeding, brains were prepared and subjected to two-step lipid extraction and shotgun lipidomics. The complete lipidomic dataset involving the different diets is displayed in Table S1. We hypothesized that feeding mice with dietary lipids from conception onward would result in more profound differences compared with adult-fed mice. Surprisingly, the lipid-class distribution did not significantly differ between the two feeding schemes (Figure 6; Figures S7E–S7G). Although the difference between mice fed diets composed of 5% beef tallow and those whose diets had 5% safflower oil was minor, the diet containing 5% fish oil led to the largest differences, especially among GPLs (Figure 6A). In particular, lipid species and subspecies of PE and PE O- were distributed differently (Figures 6B and 6C). Interestingly, the molar percentage of PE subspecies containing 4 DBs was significantly lower in the fish-oil-treated group, whereas the molar content of PE subspecies with 6 DBs was higher (Figure 6B), which correlates to the higher amount of n-3 fatty acids in this diet. In addition, a similar shift toward higher numbers of DBs in the acyl chains was detected in PE O- subspecies. Here, we were able to observe fewer subspecies with 5 DBs and an increase of subspecies with 7 DBs in animals fed a diet containing 5% fish oil (Figure 6C). The ratio of n-6/n-3 fatty acids is lower in fish oil compared with safflower oil and beef-tallow-substituted diets; therefore, we analyzed the concentration of lipid species within the predominant GPL classes, including PE, PE O-, PC, PC O-, and PS, containing at least one 20:4, 20:5, or 22:6 acyl chain, because these residues include n-6 (20:4) and n-3 (20:5 and 22:6) fatty acids. Summing up the molar concentration of these species reveals that the content of GPL species containing 20:4 acyl chains is lower in the fish-oil-treated group, whereas the concentration of lipids containing 22:6 (and 20:5) acyl chains increases (Figure 6D).

Lipidomics of Mouse Brain Regions in Aged, Apolipoprotein-E-Deficient, and APP/PS1 Transgenic Mice

Next, we aimed to determine how the brain lipidome changes during aging. Electron microscopy studies performed in mice and primates have revealed that major structural alterations that occur during aging consist of myelin degeneration within the white matter (Peters, 2002; Safaiyan et al., 2016). To determine associated changes in the lipidome, we focused on the corpus callosum and the prefrontal cortex as white and gray matter areas, respectively. We analyzed the prefrontal cortex and corpus callosum lipidome of the aging brain and compared the lipid profiles to those obtained from mice deficient in apolipoprotein E (ApoE), the major lipoprotein in the brain with an important role in age-related neurodegenerative diseases such as Alzheimer's disease (Di Paolo and Kim, 2011; Wong et al., 2017) (Figures 7A–7E). Furthermore, we evaluated the brain lipidome of transgenic β-amyloid precursor protein (APP)/presenilin-1 (PS1) mice, overexpressing human mutant forms (APP^{751SL} and $PS1^{M146L}$), which serve as a mouse model of Alzheimer's disease and are known to be genetically linked to disturbances of lipid metabolisms (Jankowsky et al., 2004) (Figures 7F and 7G). The entire lipidome datasets are displayed in Table S1. When we quantified lipid classes, we did not detect significant differences (data not shown); however, when lipid species and subspecies were determined, changes in regional patterns were found. As visualized in the heatmaps, age-associated lipidome changes were seen in both the corpus callosum and the prefrontal cortex of 6- and 20-month-old wild-type mice (Figure 7A). The lipid species composition of old (20 months) versus young (6 months) mice and wild-type versus ApoE knockout (KO) mice was analyzed by multiple-comparison tests for significant differences (Figure 7C). PE O- composition showed marked age-associated variability, for example, with an increase in PE O− 18:2;0/18:1;0 in both the corpus callosum and the prefrontal cortex (Figures 7C and 7D). HexCer species, known to be enriched in myelin, varied greatly in the corpus callosum. For example, HexCer 42:1;3 levels were reduced, whereas the amount of HexCer 42:2;3 was increased in 20-month-old compared with 6-month-old wild-type mice (Figures 7C and 7E). In addition, a substantial increase in HexCer 42:2;3 and HexCer 40:1;3 was detected in the prefrontal cortex of aged mice (Figures 7C and 7E). When analyzing the lipidome profiles of 6- and 20-month-old ApoE-deficient mice and comparing these with the profiles of aged-matched wild-type mouse brains, we observed changes in the regional lipid composition, as shown in the heatmaps (Figure 7B). Again, we found changes in HexCer species composition particularly in the corpus callosum (Figures 7C and 7E). For example, HexCer 40:1;3 and 42:2;3 were detected in higher amounts in ApoE KO compared with wild type (Figures 7C and 7E). Phospholipids were also changed, for example, with an increase in various PE O− species in ApoE-deficient mice (Figures 7C and 7D).

We also analyzed the lipidome of APP/PS1 transgenic mice in the corpus callosum and prefrontal cortex at the age of 20 weeks and compared the lipid profiles with those of wild-type littermates. Differences of the lipid composition are illustrated as a heatmap in Figure 7F. Varying lipid profiles were found predominantly among phospholipid species such as PC and PE and their ether-linked lipid species. Again, changes in lipid profiles were region

Figure 4. Lipid-Class Composition of Distinct Mouse Brain Regions

(A) Heatmap representing color-coded *Z* scores of lipid-class distribution of the 13 most abundant lipid classes of 10 brain regions. Data are in percentage of moles with mean and standard deviation. Lipid class is indicated above each graph.

(B) Differences of concentration of individual lipid classes in distinct brain regions. Data are in percentage of moles with mean and standard deviation. Lipid class is indicated above each graph.

(C) Exemplary demonstration of heterogeneous lipid-class distribution in optic nerve versus prefrontal cortex. Data shown as the percentage of moles difference from the average for abundant lipid classes.

n = 3 for all brain regions, except n = 4 for brain stem, cerebellum, and olfactory bulb. Lipid classes are defined by Lipid Maps classification (Table S2). See also Figures S1–S3 and Table S1.

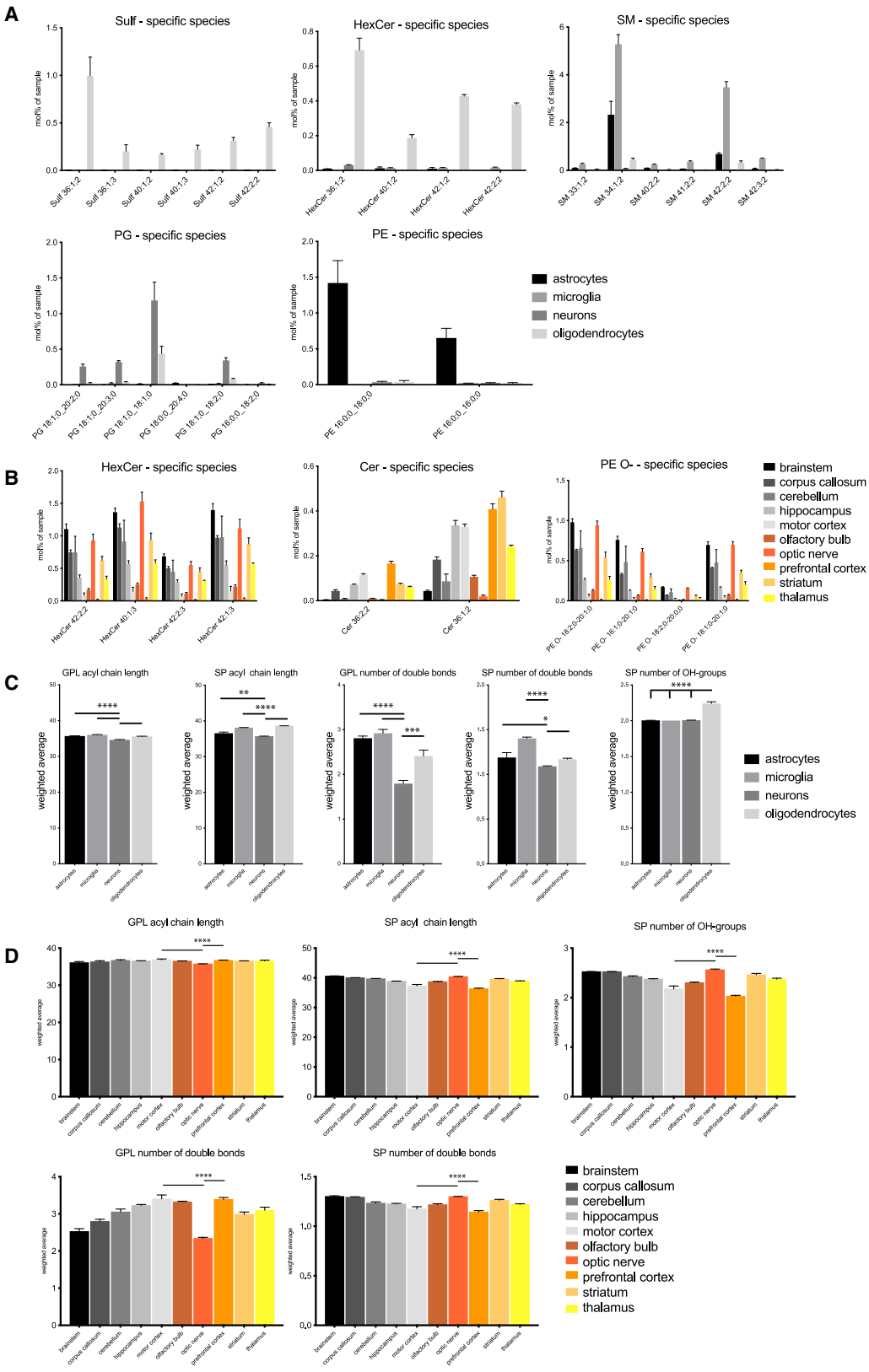

(legend on next page)

dependent, for example, with an increase of PC O− species 16:0;0/16:0;0 and 16:0;0/18:1;0 in the prefrontal cortex and a decrease of PC O− species 0-17:0;0/20:2;0 and 0-17:1;0/20:1;0 in the corpus callosum of APP/PS1 transgenic mice (Figure 7G).

DISCUSSION

We generated a cell-type- and brain-region-resolved quantitative lipid analysis of the mouse brain, quantified more than 700 lipid species in 24 lipid classes, and characterized fatty acid chain length and saturation, as well as number of OH groups. We generated lipid profiles of neurons, oligodendrocytes, astrocytes, and microglia that revealed unique lipid-class signatures and cell-specific lipid species, such as enrichment of Sulf and HexCer in oligodendrocytes; Chol and Cer in neurons; PS, PI, and DAG in astrocytes; and SM and PG in microglia. Although differences in the abundance of lipid classes among cell types were relatively modest, we found lipid species that were elevated more than 20-fold in the different cell types. In addition, we were able to detect remarkable differences in the regional lipid composition of different brain regions with variations of their lipid-class and species profiles. Although the lipid composition of the vertebrate CNS is relatively conserved, an increasing complexity of mammalian CNS during evolution is accompanied by a growing specialization of CNS lipid species (Bozek et al., 2015). Yet the reasons for this high diversity of lipids are poorly understood. In contrast to proteomic and transcriptomic approaches, by which biological function and underlying cellular mechanisms can frequently be studied through analysis of a defined subset of protein or RNA expression levels, lipid-mediated processes are rarely determined by distinct subsets of lipid species; rather, they are determined by changes in lipid profiles affecting the concentration of species on a range (Muro et al., 2014). Therefore, we aimed to obtain deeper insight into CNS lipid profiles by including cell-type- and brain-region-resolved proteomic data and found that lipid profiles can be differentiated by inclusion of concomitant evaluation of protein expression levels. For example, in our dataset, we found that microglia are enriched in SPs and that many biological processes associated with SP metabolism, including regulation of SP biosynthesis, sphinganine-1-phosphate biosynthesis, SP translocation, and catabolism, are found in microglia. Clustering of steroid-related pathways revealed that pathways associated with sterol biosynthesis are overrepresented in neurons and oligodendrocytes, whereas sterol storage and the efflux pathway are assigned to microglia. One possible limitation is that quantification of the lipid composition of mature CNS cell types requires the use of cell-type-specific differentiation media with varying formulations of serum supplements, which might additionally modulate the lipid profiles of the cultured CNS cell types. In addition, brain-region-related differences of lipid composition are accompanied by regional patterns of lipid-related proteomic pathways. Nevertheless, our integration of lipidome and proteome data is useful to obtain deeper insights into the various functions of the detected lipids and their associated metabolic networks. These networks can change not only in the course of various diseases but also in response to different diets (Frahnow et al., 2017; Giles et al., 2016; Pati et al., 2018). We used diets containing different mixtures of lipids to measure differences, in particular, of polyunsaturated fatty acids, which have an essential function in the normal development and functioning of the CNS (Harauma et al., 2017; Hanna and Hafez, 2018; Yang et al., 2019). We found that diets with differences in fatty acid saturation (beef tallow and safflower) resulted in only minor differences in the brain lipidome, whereas diets enriched in the n-3 fatty acids, eicosapentaenoic acid (EPA) and docosahexaenoic acid (DHA) (fish oil), gave rise to significant alterations in the phospholipid fatty acid composition. Remarkably, similar differences were detected in adult-fed mice, pointing to relatively fast turnover and the possibility of efficient dietary interventions in adults. Arachidonic acid (AA), EPA, and DHA have high clinical interest, because they are precursors of lipid mediators such as eicosanoids involved in inflammatory response (Melo et al., 2019). AA is a precursor of pro-inflammatory eicosanoids, whereas EPA and DHA are precursors of pro-resolving mediators with important roles in inflammation resolution (Dennis and Norris, 2015; Tessaro et al., 2015). Our lipid-related pathways and biological function analysis showed that microglia are enriched in processes regulating prostaglandin and arachidonic metabolism. Thus, dietary changes of AA, EPA, and DHA may directly modulate microglial features, which would be of relevance for inflammatory diseases and for neurodegenerative CNS diseases associated with inflammation.

Many studies have discovered that lipids are associated with age-related neurodegenerative diseases such as Alzheimer's disease, in which loss of ether-linked phospholipids (plasmalogens) and Sulf have been documented (Han et al., 2001, 2002). Plasmalogen deficiency could be a result of increased oxidative stress, as plasmalogens can act as sacrificial oxidants. Additionally, changes in myelin ultrastructure, a membrane enriched in

Figure 5. Enrichment of Lipid Species in Certain Cell Types or Tissue Regions

(A) Lipid species of five lipid classes (Sulf, HexCer, SM, PG, and PE, as labeled above the graphs) demonstrating highly enriched content of selected species in percentage of moles in oligodendrocytes (Sulf and HexCer species), microglia (SM species), neurons (PG species), or astrocytes (PE species).

(B) Lipid species of three lipid classes (HexCer, Cer, and PE O-, as labeled above the graphs) demonstrating localized enrichment in percentage of moles of selected species in certain brain regions.

(C) Features of GPL and SP fatty acids in various CNS cell types displayed as the weighted average of GPL and SP fatty acid chain length in number of C atoms, number of DBs in GPL and SP, and number of OH groups in SP. The relevant feature is indicated above each graph.

(D) Features of GPL and SP fatty acids in various brain regions displayed as the weighted average of GPL and SP fatty acid chain length in number of C atoms, number of DBs in GPL and SP, and number of OH groups in SP. The relevant feature is indicated above each graph.

Mean with standard deviation (n = 3 for cell types and brain regions, except n = 4 for brain stem, cerebellum, and olfactory bulb). The weighted average was calculated by weighing with the molar concentration of the relevant lipid category. Lipid categories are SP and GPL, with lipid classes defined by Lipid Maps classification (Table S2). *$p < 0.05$, **$p < 0.01$, ***$p < 0.001$, ****$p < 0.0001$, p values by multiple-comparison test (Tukey). See also Figures S4–S7 and Tables S1, S5, and S6.

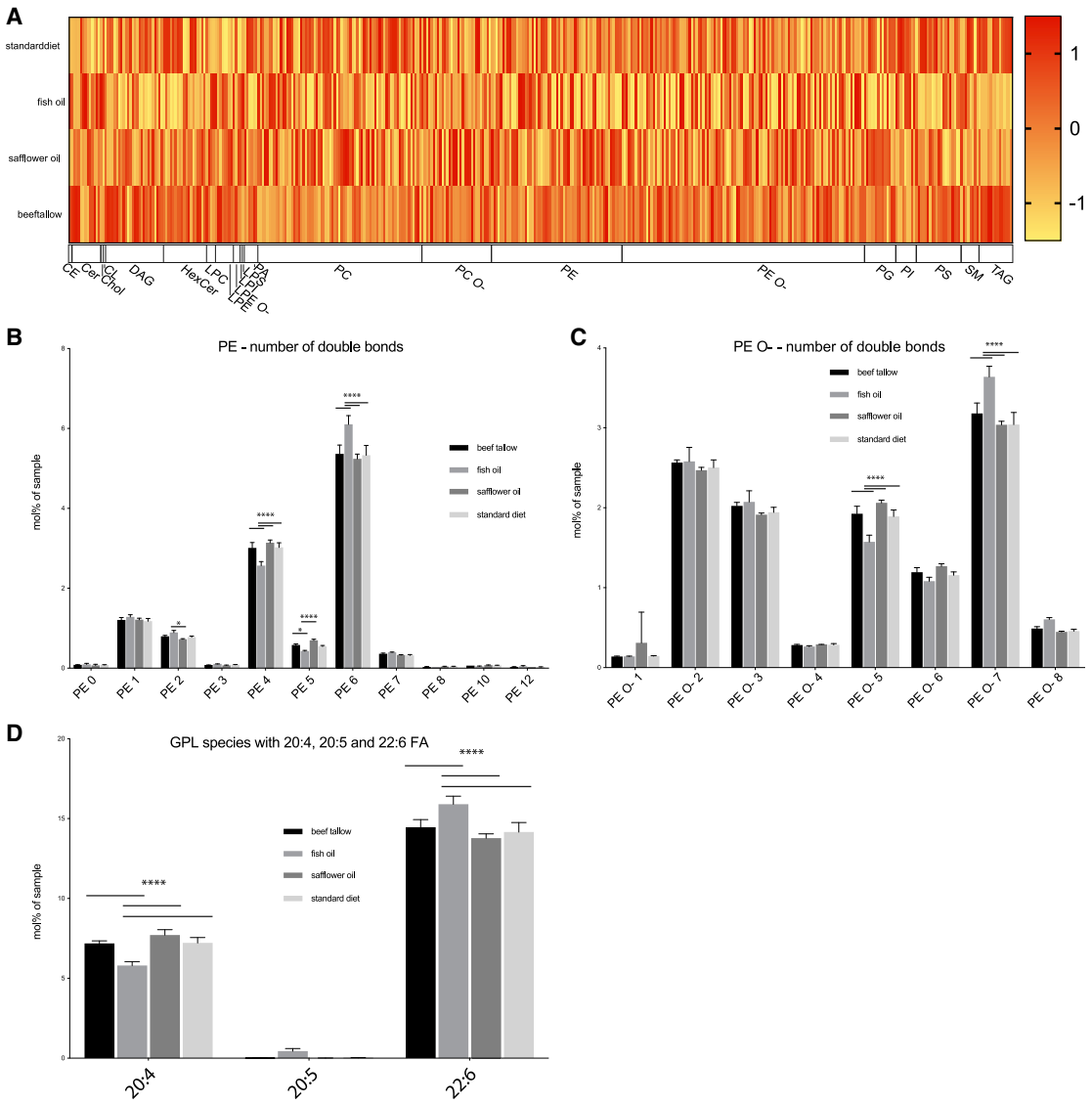

Figure 6. Effects of Diets on the Adult Brain Lipidome

(A) Heatmap representing color-coded *Z* scores of lipid subspecies distribution clustered by lipid classes in whole-brain samples of adult mice fed a standard diet or a diet enriched with fish oil, safflower oil, or beef tallow.

(B and C) Molar concentration of (B) PE species or (C) PE O- species in relation to the number of total DBs in both fatty acid acyl chains of these species.

(D) Molar concentration of glycerophospholipids (GPL) containing at least one fatty acid (FA) with a 20:4, 20:5, or 22:6 configuration.

Hemispheric brain samples of adult mice fed diets containing beef tallow, fish oil, safflower oil, or a standard diet analyzed by shotgun lipidomics and compared (n = 5 for each diet). Mean with standard deviation in (B-D). Lipid classes are as defined by Lipid Maps classification (Table S2). *p < 0.05, ****p < 0.0001, p values by multiple-comparison test (Tukey). See also Figure S7 and Table S1.

plasmalogens, are conceivable. In our study, we quantified lipids in both gray and white matter, because aging is associated with major ultrastructural alterations, particularly in myelin within the white matter (Peters, 2002). Consistent with age-related myelin changes, we detected differences in HexCer and PE O- species, two lipid classes particularly enriched in myelin. These results are consistent with dysregulated lipid metabolism in the aging brain (Söderberg et al., 1990; Tu et al., 2017), and a further understanding of such age-related alterations of lipid profiles is important, because aging is a major risk factor for the most prevalent neurodegenerative diseases. In our study, we used shotgun lipidomics, which allows absolute quantification of entire lipid profiles; however, there are limitations of this method, which include difficulty in resolving isobaric species, such as glucosyl- and galactosylceramide, and very low abundant lipids. Although our dataset provides an initial snapshot of the lipid composition in the brain that can serve as a resource for understanding brain development and function, more work is required to extend the

CellPress
OPEN ACCESS

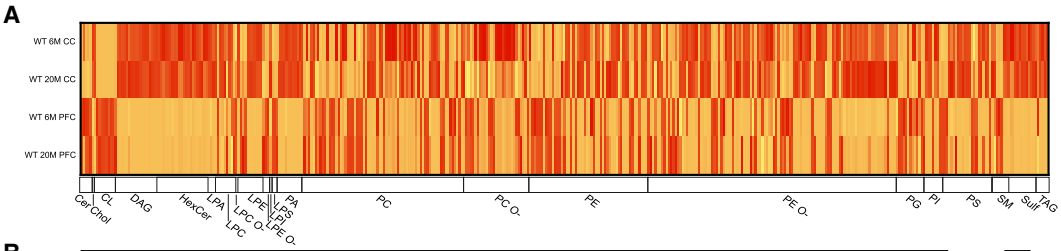

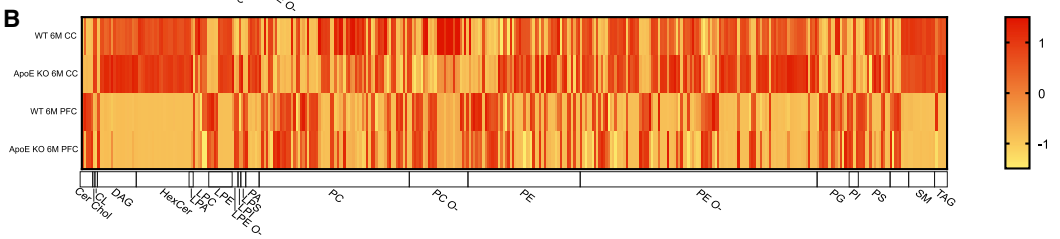

C

	corpus callosum			prefrontal cortex		
	WT vs. ApoE KO 6months	WT vs. ApoE KO 20months	WT 6M vs. 20M	WT vs. ApoE KO 6months	WT vs. ApoE KO 20months	WT 6M vs. 20M
	mol%	mol%	mol%	mol%	mol%	mol%
Cer 36:1;2					0,023 *	0,019 *
HexCer 42:2;3	-0,208 **		-0,242 ***			
HexCer 40:1;3	-0,177 *					-0,100 ****
HexCer 42:1;3			0,339 ****			
HexCer 42:2;2	-0,198 **	-0,184 *				
HexCer 42:2;3						-0,072 **
PC 16:0;0_16:0;0			0,406 **			0,227 ****
PC 16:0;0_18:0;0						0,144 **
PC 16:0;0_18:1;0	-0,626 ***	-0,354 *			0,554 ****	-0,157 **
PC 16:0;0_22:6;0					0,198 ***	
PC 16:1;0_16:1;0				0,389 ****		0,142 *
PC 17:0;0_20:1;0	0,535 ***					
PC 18:0;0_18:1;0			0,324 *	-0,203 ****	-0,141 *	
PC 18:0;0_20:4;0					-0,157 **	
DAG 16:0;0_18:1;0	-0,098 ****	-0,104 ****				
DAG 18:0;0_18:1;0	-0,105 ****	-0,108 ****				
DAG 18:0;0_20:4;0	-0,057 ****	-0,044 **	-0,040 **			
DAG 18:1;0_18:1;0	-0,035 *	-0,039 *				
LPA 16:2;0	-0,025 **					
LPE O- 0-18:2;0	-0,002 *		-0,004 ****			
PC O- 0-16:1;0/16:0;0						0,008 **
PC O- 0-17:0;0/20:2;0	0,411 ***		0,425 ***			
PC O- 0-17:1;0/20:1;0	0,282 *		0,274 *			
PC O- 0-18:1;0/16:0;0				0,006 *	0,009 ***	
PE 18:0;0_18:1;0	-0,171 ****	-0,216 ****				
PE 18:0;0_20:4;0	-0,361 ****	-0,175 ****		-0,328 ****	-0,541 ****	
PE 18:0;0_22:4;0	-0,096 *					
PE 18:0;0_22:6;0	-0,272 ****		0,120 **		0,708 ****	
PE 18:1;0_18:1;0			-0,104 *			
PE O- 0-16:1;0/20:4;0				-0,058 *	-0,061 *	
PE O- 0-16:1;0/22:4;0				-0,100 ****	-0,137 ****	
PE O- 0-16:1;0/22:6;0				-0,103 ****	-0,055 *	
PE O- 0-18:1;0/18:1;0	-0,102 **	-0,204 ****	0,220 ****			
PE O- 0-18:1;0/20:1;0	-0,101 *	-0,118 **				
PE O- 0-18:1;0/20:4;0				-0,117 ****	-0,127 ****	0,077 ***
PE O- 0-18:1;0/22:4;0			0,098 *	-0,087 ****	-0,090 ***	
PE O- 0-18:1;0/22:6;0	-0,095 *		0,116 **	-0,166 ****		0,157 ****
PE O- 0-18:2;0/18:1;0	-0,483 ****	-0,284 ****	-0,850 ****			-0,082 ***
PE O- 0-18:2;0/20:1;0	-0,320 ****	-0,196 ****	-0,464 ****			
PE O- 0-18:2;0/20:4;0	-0,107 **		-0,183 ****			-0,055 *
PE O- 0-18:2;0/22:4;0	-0,096 *		-0,106 **			
PE O- 0-18:2;0/22:6;0						-0,065 **
PG 16:0;0_18:1;0	-0,011 ****	-0,008 **				0,010 *
PG 18:0;0_20:4;0						0,010 *
PG 22:6;0_22:6;0						-0,017 ***
PS 18:0;0_18:1;0		0,544 ****	-0,874 ****			
SM 36:1;2	-0,097 *			-0,123 *		
Sulf 42:1;2			0,125 ****			
Sulf 42:2;2		0,106 **	-0,188 ****			
Sulf 42:2;3			-0,098 **			

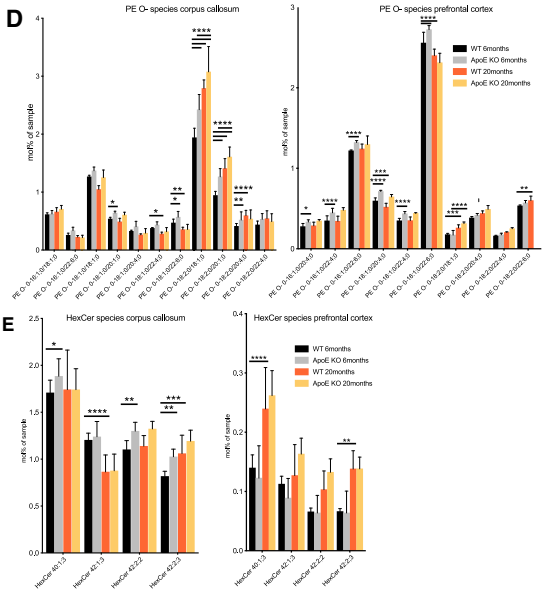

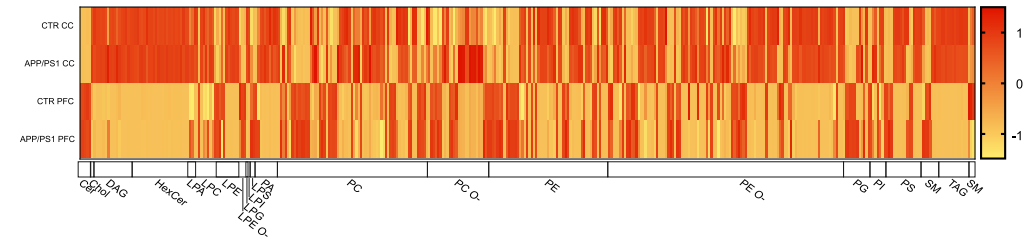

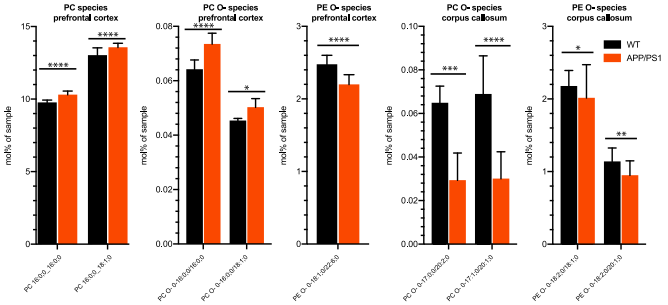

(legend on next page)

analysis to additional lipid species and to understand the relevance of these lipid profiles.

STAR★METHODS

Detailed methods are provided in the online version of this paper and include the following:

- KEY RESOURCES TABLE
- RESOURCE AVAILABILITY
  - Lead Contact
  - Materials Availability
  - Data and Code Availability
- EXPERIMENTAL MODEL AND SUBJECT DETAILS
  - Mice
  - Tissue preparation, cell culture and cell isolation
- METHOD DETAILS
  - Annotation of lipid classes and species
  - Lipid extraction for mass spectrometry lipidomics
  - MS data acquisition
- QUANTIFICATION AND STATISTICAL ANALYSIS
  - Data analysis and post-processing
  - Lipidome-related mouse brain proteome analysis

SUPPLEMENTAL INFORMATION

Supplemental Information can be found online at https://doi.org/10.1016/j.celrep.2020.108132.

ACKNOWLEDGMENTS

The work was supported by grants from the German Research Foundation (SPP2191, TRR128-2, and TRR274-1) and SyNergy Excellence Cluster EXC2145 (project 390857198), the Human Frontier Science Program (HFSP), the ERC (consolidator grant to M. Simons), and the Dr. Miriam and Sheldon G. Adelson Medical Research Foundation. We thank Constanze Depp for providing APP/PS1 transgenic mice.

AUTHOR CONTRIBUTIONS

D.F. and M. Simons conceived the project and designed experiments. D.F., H.P., M.A.S., C.K., C.G.B., M. Su, M.-T.W., and J.M.B. carried out experiments. D.F., C.K., J.M.B., and M.M. analyzed the data or supervised data acquisition or analysis. D.F. and J.M.B. visualized the data. D.F. and M. Simons supervised the project and wrote the manuscript.

DECLARATION OF INTERESTS

M.A.S. and C.K. are employees and shareholders of Lipotype.

Received: November 18, 2019
Revised: July 1, 2020
Accepted: August 20, 2020
Published: September 15, 2020

REFERENCES

Aureli, M., Grassi, S., Prioni, S., Sonnino, S., and Prinetti, A. (2015). Lipid membrane domains in the brain. Biochim Biophys Acta *1851*, 1006–1016.

Bozek, K., Wei, Y., Yan, Z., Liu, X., Xiong, J., Sugimoto, M., Tomita, M., Pääbo, S., Sherwood, C.C., Hof, P.R., et al. (2015). Organization and evolution of brain lipidome revealed by large-scale analysis of human, chimpanzee, macaque, and mouse tissues. Neuron *85*, 695–702.

Butovsky, O., and Weiner, H.L. (2018). Microglial signatures and their role in health and disease. Nat. Rev. Neurosci. *19*, 622–635.

Camargo, N., Goudriaan, A., van Deijk, A.F., Otte, W.M., Brouwers, J.F., Lodder, H., Gutmann, D.H., Nave, K.-A., Dijkhuizen, R.M., Mansvelder, H.D., et al. (2017). Oligodendroglial myelination requires astrocyte-derived lipids. PLoS Biol. *15*, e1002605.

Chrast, R., Saher, G., Nave, K.-A., and Verheijen, M.H.G. (2011). Lipid metabolism in myelinating glial cells: lessons from human inherited disorders and mouse models. J. Lipid Res. *52*, 419–434.

Davie, K., Janssens, J., Koldere, D., De Waegeneer, M., Pech, U., Kreft, Ł., Aibar, S., Makhzami, S., Christiaens, V., Bravo González-Blas, C., et al. (2018). A Single-Cell Transcriptome Atlas of the Aging *Drosophila* Brain. Cell *174*, 982–998.e20.

Dawson, G. (2015). Measuring brain lipids. Biochim. Biophys. Acta *1851*, 1026–1039.

Deczkowska, A., Keren-Shaul, H., Weiner, A., Colonna, M., Schwartz, M., and Amit, I. (2018). Disease-Associated Microglia: A Universal Immune Sensor of Neurodegeneration. Cell *173*, 1073–1081.

Dennis, E.A., and Norris, P.C. (2015). Eicosanoid storm in infection and inflammation. Nat. Rev. Immunol. *15*, 511–523.

Di Paolo, G., and Kim, T.-W. (2011). Linking lipids to Alzheimer's disease: cholesterol and beyond. Nat. Rev. Neurosci. *12*, 284–296.

Figure 7. Lipidomics of Mouse Brain Regions in Aged, ApoE-Deficient (ApoE KO), and APP/PS1 Transgenic Mice

(A) Heatmap representing color-coded *Z* scores of lipid subspecies distribution clustered by lipid classes in the corpus callosum (CC) and the prefrontal cortex (PFC) of wild-type mice at the ages of 6 and 20 months.

(B) Heatmap representing color-coded *Z* scores of lipid subspecies distribution clustered by lipid classes in CC and PFC of wild-type (WT) and ApoE KO mice at the age of 6 months.

(C) Table displaying results of a statistical analysis by multiple-comparison test (Tukey). Significant differences in lipid subspecies concentration in either CC or PFC between WT mice at the age of 6 months and those at 20 months or WT and ApeE KO mice at the age of either 6 or 20 months are displayed. Values represent the average difference of the lipid subspecies amounts in percentage of moles. Increased amounts are labeled yellow, decreased amounts are labeled red, and p values are indicated by stars (*$p < 0.05$, **$p < 0.01$, ***$p < 0.001$, ****$p < 0.0001$).

(D and E) Exemplary illustration of lipid species amounts in percentage of moles of (D) PE O− species or (E) HexCer species in CC or PFC of WT mice or ApoE KO mice at the ages of 6 and 20 months. Data are in percentage of moles of the sample, mean with standard deviation; *$p < 0.05$, **$p < 0.01$, ***$p < 0.001$, ****$p < 0.0001$, p values by multiple-comparison test (Tukey).

(F) Heatmap representing color-coded *Z* scores of lipid subspecies distribution clustered by lipid classes in CC and PFC of WT littermates (CTR) and APP/PS1 transgenic mice at the age of 20 weeks.

(G) Graphs displaying exemplary lipid species of 3 lipid classes (PC, PC O−, and PE O−, as labeled above the graphs) demonstrating the amount in percentage of moles in either WT or APP/PS1 mice. Data are in percentage of moles of the sample, mean with standard deviation (n = 4 for WT mice aged 6 and 20 months, n = 3 for ApoE KO mice aged 6 and 20 months, n = 4 for APP/PS1, and n = 3 for WT littermates); *$p < 0.05$, **$p < 0.01$, ***$p < 0.001$, ****$p < 0.0001$, p values by multiple-comparison test (Sidak).

Lipid classes are defined by Lipid Maps classification (Table S2). See also Table S1.

Ejsing, C.S., Sampaio, J.L., Surendranath, V., Duchoslav, E., Ekroos, K., Klemm, R.W., Simons, K., and Shevchenko, A. (2009). Global analysis of the yeast lipidome by quantitative shotgun mass spectrometry. Proc. Natl. Acad. Sci. USA *106*, 2136–2141.

Fahy, E., Subramaniam, S., Murphy, R.C., Nishijima, M., Raetz, C.R.H., Shimizu, T., Spener, F., van Meer, G., Wakelam, M.J.O., and Dennis, E.A. (2009). Update of the LIPID MAPS comprehensive classification system for lipids. J. Lipid Res. *50* (*Suppl*), S9–S14.

Fitzner, D., Schnaars, M., van Rossum, D., Krishnamoorthy, G., Dibaj, P., Bakhti, M., Regen, T., Hanisch, U.-K., and Simons, M. (2011). Selective transfer of exosomes from oligodendrocytes to microglia by macropinocytosis. J. Cell Sci. *124*, 447–458.

Frahnow, T., Osterhoff, M.A., Hornemann, S., Kruse, M., Surma, M.A., Klose, C., Simons, K., and Pfeiffer, A.F.H. (2017). Heritability and responses to high fat diet of plasma lipidomics in a twin study. Sci. Rep. *7*, 3750.

Giles, C., Takechi, R., Mellett, N.A., Meikle, P.J., Dhaliwal, S., and Mamo, J.C. (2016). The Effects of Long-Term Saturated Fat Enriched Diets on the Brain Lipidome. PLoS ONE *11*, e0166964.

Gross, R.W. (2017). The evolution of lipidomics through space and time. Biochim. Biophys. Acta Mol. Cell Biol. Lipids *1862*, 731–739.

Han, X., Holtzman, D.M., and McKeel, D.W., Jr. (2001). Plasmalogen deficiency in early Alzheimer's disease subjects and in animal models: molecular characterization using electrospray ionization mass spectrometry. J. Neurochem. *77*, 1168–1180.

Han, X., M Holtzman, D., McKeel, D.W., Jr., Kelley, J., and Morris, J.C. (2002). Substantial sulfatide deficiency and ceramide elevation in very early Alzheimer's disease: potential role in disease pathogenesis. J. Neurochem. *82*, 809–818.

Hanna, V.S., and Hafez, E.A.A. (2018). Synopsis of arachidonic acid metabolism: A review. J. Adv. Res. *11*, 23–32.

Harauma, A., Hatanaka, E., Yasuda, H., Nakamura, M.T., Salem, N., Jr., and Moriguchi, T. (2017). Effects of arachidonic acid, eicosapentaenoic acid and docosahexaenoic acid on brain development using artificial rearing of delta-6-desaturase knockout mice. Prostaglandins Leukot. Essent. Fatty Acids *127*, 32–39.

Harayama, T., and Riezman, H. (2018). Understanding the diversity of membrane lipid composition. Nat. Rev. Mol. Cell Biol. *19*, 281–296.

Hawrylycz, M.J., Lein, E.S., Guillozet-Bongaarts, A.L., Shen, E.H., Ng, L., Miller, J.A., van de Lagemaat, L.N., Smith, K.A., Ebbert, A., Riley, Z.L., et al. (2012). An anatomically comprehensive atlas of the adult human brain transcriptome. Nature *489*, 391–399.

Heiman, M., Schaefer, A., Gong, S., Peterson, J.D., Day, M., Ramsey, K.E., Suárez-Fariñas, M., Schwarz, C., Stephan, D.A., Surmeier, D.J., et al. (2008). A translational profiling approach for the molecular characterization of CNS cell types. Cell *135*, 738–748.

Herzog, R., Schwudke, D., Schuhmann, K., Sampaio, J.L., Bornstein, S.R., Schroeder, M., and Shevchenko, A. (2011). A novel informatics concept for high-throughput shotgun lipidomics based on the molecular fragmentation query language. Genome Biol. *12*, R8.

Herzog, R., Schuhmann, K., Schwudke, D., Sampaio, J.L., Bornstein, S.R., Schroeder, M., and Shevchenko, A. (2012). LipidXplorer: a software for consensual cross-platform lipidomics. PLoS ONE *7*, e29851.

Ingólfsson, H.I., Carpenter, T.S., Bhatia, H., Bremer, P.-T., Marrink, S.J., and Lightstone, F.C. (2017). Computational Lipidomics of the Neuronal Plasma Membrane. Biophys. J. *113*, 2271–2280.

Jankowsky, J.L., Fadale, D.J., Anderson, J., Xu, G.M., Gonzales, V., Jenkins, N.A., Copeland, N.G., Lee, M.K., Younkin, L.H., Wagner, S.L., et al. (2004). Mutant presenilins specifically elevate the levels of the 42 residue beta-amyloid peptide *in vivo*: evidence for augmentation of a 42-specific gamma secretase. Hum. Mol. Genet. *13*, 159–170.

Khakh, B.S., and Deneen, B. (2019). The Emerging Nature of Astrocyte Diversity. Annu. Rev. Neurosci. *42*, 187–207.

Lauwers, E., Goodchild, R., and Verstreken, P. (2016). Membrane Lipids in Presynaptic Function and Disease. Neuron *90*, 11–25.

Liebisch, G., Binder, M., Schifferer, R., Langmann, T., Schulz, B., and Schmitz, G. (2006). High throughput quantification of cholesterol and cholesteryl ester by electrospray ionization tandem mass spectrometry (ESI-MS/MS). Biochim. Biophys. Acta *1761*, 121–128.

Mahfouz, A., Huisman, S.M.H., Lelieveldt, B.P.F., and Reinders, M.J.T. (2017). Brain transcriptome atlases: a computational perspective. Brain Struct. Funct. *222*, 1557–1580.

Melo, H.M., Santos, L.E., and Ferreira, S.T. (2019). Diet-Derived Fatty Acids, Brain Inflammation, and Mental Health. Front. Neurosci. *13*, 265.

Muro, E., Atilla-Gokcumen, G.E., and Eggert, U.S. (2014). Lipids in cell biology: how can we understand them better? Mol. Biol. Cell *25*, 1819–1823.

Pati, S., Krishna, S., Lee, J.H., Ross, M.K., de La Serre, C.B., Harn, D.A., Jr., Wagner, J.J., Filipov, N.M., and Cummings, B.S. (2018). Effects of high-fat diet and age on the blood lipidome and circulating endocannabinoids of female C57BL/6 mice. Biochim. Biophys. Acta Mol. Cell Biol. Lipids *1863*, 26–39.

Peters, A. (2002). The effects of normal aging on myelin and nerve fibers: a review. J. Neurocytol. *31*, 581–593.

Piedrahita, J.A., Zhang, S.H., Hagaman, J.R., Oliver, P.M., and Maeda, N. (1992). Generation of mice carrying a mutant apolipoprotein E gene inactivated by gene targeting in embryonic stem cells. Proc. Natl. Acad. Sci. USA *89*, 4471–4475.

Safaiyan, S., Kannaiyan, N., Snaidero, N., Brioschi, S., Biber, K., Yona, S., Edinger, A.L., Jung, S., Rossner, M.J., and Simons, M. (2016). Age-related myelin degradation burdens the clearance function of microglia during aging. Nat. Neurosci. *19*, 995–998.

Saher, G., Brügger, B., Lappe-Siefke, C., Möbius, W., Tozawa, R., Wehr, M.C., Wieland, F., Ishibashi, S., and Nave, K.-A. (2005). High cholesterol level is essential for myelin membrane growth. Nat. Neurosci. *8*, 468–475.

Sampaio, J.L., Gerl, M.J., Klose, C., Ejsing, C.S., Beug, H., Simons, K., and Shevchenko, A. (2011). Membrane lipidome of an epithelial cell line. Proc. Natl. Acad. Sci. USA *108*, 1903–1907.

Santello, M., Toni, N., and Volterra, A. (2019). Astrocyte function from information processing to cognition and cognitive impairment. Nat. Neurosci. *22*, 154–166.

Schmitt, S., Castelvetri, L.C., and Simons, M. (2015). Metabolism and functions of lipids in myelin. Biochim. Biophys. Acta *1851*, 999–1005.

Sharma, K., Schmitt, S., Bergner, C.G., Tyanova, S., Kannaiyan, N., Manrique-Hoyos, N., Kongi, K., Cantuti, L., Hanisch, U.-K., Philips, M.-A., et al. (2015). Cell type- and brain region-resolved mouse brain proteome. Nat. Neurosci. *18*, 1819–1831.

Simopoulos, A.P. (2008). The importance of the omega-6/omega-3 fatty acid ratio in cardiovascular disease and other chronic diseases. Exp. Biol. Med. (Maywood) *233*, 674–688.

Skinnider, M.A., Squair, J.W., and Foster, L.J. (2019). Evaluating measures of association for single-cell transcriptomics. Nat. Methods *16*, 381–386.

Söderberg, M., Edlund, C., Kristensson, K., and Dallner, G. (1990). Lipid compositions of different regions of the human brain during aging. J. Neurochem. *54*, 415–423.

Stadelmann, C., Timmler, S., Barrantes-Freer, A., and Simons, M. (2019). Myelin in the Central Nervous System: Structure, Function, and Pathology. Physiol. Rev. *99*, 1381–1431.

Surma, M.A., Herzog, R., Vasilj, A., Klose, C., Christinat, N., Morin-Rivron, D., Simons, K., Masoodi, M., and Sampaio, J.L. (2015). An automated shotgun lipidomics platform for high throughput, comprehensive, and quantitative analysis of blood plasma intact lipids. Eur. J. Lipid Sci. Technol. *117*, 1540–1549.

Tessaro, F.H.G., Ayala, T.S., and Martins, J.O. (2015). Lipid mediators are critical in resolving inflammation: a review of the emerging roles of eicosanoids in diabetes mellitus. BioMed Res. Int. *2015*, 568408.

Tietz, S., and Engelhardt, B. (2015). Brain barriers: Crosstalk between complex tight junctions and adherens junctions. J. Cell Biol. *209*, 493–506.

Tu, J., Yin, Y., Xu, M., Wang, R., and Zhu, Z.-J. (2017). Absolute quantitative lipidomics reveals lipidome-wide alterations in aging brain. Metabolomics *14*, 5.

Tyanova, S., Temu, T., Sinitcyn, P., Carlson, A., Hein, M.Y., Geiger, T., Mann, M., and Cox, J. (2016). The Perseus computational platform for comprehensive analysis of (prote)omics data. Nat. Methods *13*, 731–740.

Wang, M., Wang, C., Han, R.H., and Han, X. (2016). Novel advances in shotgun lipidomics for biology and medicine. Prog. Lipid Res. *61*, 83–108.

Wong, M.W., Braidy, N., Poljak, A., Pickford, R., Thambisetty, M., and Sachdev, P.S. (2017). Dysregulation of lipids in Alzheimer's disease and their role as potential biomarkers. Alzheimers Dement. *13*, 810–827.

Ximerakis, M., Lipnick, S.L., Innes, B.T., Simmons, S.K., Adiconis, X., Dionne, D., Mayweather, B.A., Nguyen, L., Niziolek, Z., Ozek, C., et al. (2019). Single-cell transcriptomic profiling of the aging mouse brain. Nat. Neurosci. *22*, 1696–1708.

Yang, B., Fritsche, K.L., Beversdorf, D.Q., Gu, Z., Lee, J.C., Folk, W.R., Greenlief, C.M., and Sun, G.Y. (2019). Yin-Yang Mechanisms Regulating Lipid Peroxidation of Docosahexaenoic Acid and Arachidonic Acid in the Central Nervous System. Front. Neurol. *10*, 642.

Zhang, Y., Chen, K., Sloan, S.A., Bennett, M.L., Scholze, A.R., O'Keeffe, S., Phatnani, H.P., Guarnieri, P., Caneda, C., Ruderisch, N., et al. (2014). An RNA-sequencing transcriptome and splicing database of glia, neurons, and vascular cells of the cerebral cortex. J. Neurosci. *34*, 11929–11947.

STAR★METHODS

KEY RESOURCES TABLE

REAGENT or RESOURCE	SOURCE	IDENTIFIER
Chemicals, Peptides, and Recombinant Proteins		
Standard mouse diet (5% soybean oil)	ssniff Spezialdiäten GmbH	ssniff S7007-E020
Mouse diet with 5% beef tallow	ssniff Spezialdiäten GmbH	ssniff S7007-E022
Mouse diet with 5% safflower oil	ssniff Spezialdiäten GmbH	ssniff S7007-E021
Mouse diet with 5% fish oil	ssniff Spezialdiäten GmbH	ssniff S7007-E024
All internal lipid standards for quantitative lipidomics	Avanti® Polar Lipids	https://avantilipids.com/divisions/lipidomics/lipid-maps-ms-standards
Deposited Data		
Lipidomic datasets of cells and tissue analyzed	This paper	Table S1
Cell type– and brain region–resolved mouse brain proteomic dataset	Sharma et al., 2015	https://doi.org/10.1038/nn.4160
Experimental Models: Organisms/Strains		
Mouse: B6.129P2-*Apoe*^{tm1Unc}/J ApoE KO mice	The Jackson Laboratory	Stock No: 002052
Mouse: B6;C3-Tg(APPswe,PSEN1dE9)85Dbo/Mmjax APP/PS1 mice	The Jackson Laboratory	MMRRC Stock No: 34829-JAX
Software and Algorithms		
Adobe Illustrator CS5		https://www.adobe.com/products/illustrator.html
GraphPad Prism 7	GraphPad Software, Inc	https://www.graphpad.com/
LipidXplorer		Herzog et al., 2011, 2012
Perseus software versions 1.5.2.11 and 1.6.1.3		https://maxquant.net/perseus/
KEGG PATHWAY Database	KEGG: Kyoto Encyclopedia of Genes and Genomes	https://www.genome.jp/kegg/pathway.html
Gene Ontologies	GeneOntology	http://geneontology.org/
metabolic pathway information from pathbank	PathBank	http://pathbank.org
Other		
QExactive mass spectrometer	Thermo Scientific	https://www.thermofisher.com/us/en/home.html
TriVersa NanoMate ion source	Advion Biosciences	https://www.advion.com

RESOURCE AVAILABILITY

Lead Contact

Further information and requests for resources and reagents should be directed to and will be fulfilled by the Lead Contact, Mikael Simons (msimons@gwdg.de).

Materials Availability

All unique reagents generated in this study are available from the Lead Contact with a completed Material Transfer Agree.

Data and Code Availability

This study did not generate any code. The lipidomics datasets are provided in Table S1.

EXPERIMENTAL MODEL AND SUBJECT DETAILS

Mice

All experiments were performed in accordance with the German animal welfare law and local regulations for animal experiments. The animals were kept in 12h light dark-cycles and bred in the animal facility of the Max Planck Institute of Experimental Medicine, the University Medical Center Göttingen and the German Center for Neurodegenerative Diseases in Munich. APOE knockout animals (Piedrahita et al., 1992) were kindly provided by Tim Seidler (University of Göttingen, Germany). Heterozygous transgenic APP/PS1 mice (Jankowsky et al., 2004) and control littermates at the age of 20 weeks were kindly provided by Constanze Depp (Max

Planck Institute of Experimental Medicine). Adult, male mice at different ages (C57BL/6J) were fed either a standard diet (5% soybean oil, ssniff product no. S7007-E020) or a diet instead containing 5% beef tallow (ssniff S7007-E022), 5% safflower oil (ssniff S7007-E021) or 5% fish oil (ssniff S7007-E024), which were enriched in saturated fatty acids (FA), polyunsaturated FAs with a high n-6 content, or polyunsaturated FAs with a high n-3 content, respectively. An additional 2% of soybean oil was included in all diets. The mice (n = 5 per group) were receiving the specific diets from 6 weeks of age until 15 weeks of age when they were anesthetized with isoflurane and sacrificed by cervical dislocation for lipid analysis.

For the ''from conception'' cohort we fed pregnant female mice with the different diets from the time point of conception until weaning and the female offspring (n = 4, n = 5, n = 2 for beef tallow, safflower oil and fish oil, respectively) was kept on the diets until sacrifice at 8 weeks of age. Lipidomics of aging male wild-type mice was performed in C57BL/6J mice at the age of 6 month (n = 4) and the age of 20 months (n = 4). Lipidome analysis in ApoE-deficient mice was performed in male ApoE KO mice at the age of 6 months (n = 3) and 20 months (n = 3). Lipidome analysis from APP/PS1 transgenic mice was performed in heterozygous male animals (n = 4) and wild-type male littermates as a control (n = 3).

Tissue preparation, cell culture and cell isolation

All animal experiments were performed according to the Lower Saxony State regulations for animal experimentation. Animals were deeply anesthesized perfused with a 0,9% NaCl solution. Brain regions were dissected from P60 male C57BL/6 mice using a 'rodent brain matrix 1-mm coronal slicer (ASI Instruments) according to coordinates obtained from the Mouse Brain Library (http://www.mbl.org/) using the C57BL/6J atlas as reference. Dissected brain regions or tissue punches were weighed and transferred to 150mM ammonium bicarbonate solution. Subsequently, tissue was homogenized by sonication. The preparation of primary cell cultures was performed according to previously described protocol with modifications (Fitzner et al., 2011). Briefly, brains were removed from newborn mice (P1) were separated by midline incision and transferred into Hanks Buffered saline solution (HBSS). Under a dissection microscope, the meninges were removed and the hindbrains were discarded. A total of five brains were pooled and incubated with 0.25% trypsin/EDTA (wt/vol) at 37°C for 10 min. The tissues were washed twice with BME growth medium (supplemented with 10% fetal calf serum (FCS, vol/vol), GlutaMAX, penicillin and streptomycin) and further dissociated by trituration (ten times) using a glass pipette. The cell suspension was passed through a cell sieve and subsequently plated onto 5 PLL-coated cell culture flasks with BME growth medium. Two thirds of the growth medium were exchanged twice a week. 10 d after plating the glial mixed cultures, microglia were removed by gentle, manual shaking, leaving a culture that consists of OPCs on top of a confluent layer of astrocytes. The next day, OPCs were shaken off by hand and pelleted by centrifugation. The OPC-pellet was resuspended in Super Sato differentiation medium (high-glucose DMEM with B27-supplement, 1% horse serum (vol/vol), 110 μg ml−1 sodium pyruvate, 0.5 nM triiodo-thyronin, 0.5 μM l-thyroxin, GlutaMAX and penicillin/streptomycin). The OPC suspension was transferred into an untreated cell culture dish and incubated at 37°C for 3 min. During this time, contaminating microglia and astrocytes adhered to the culture dish, while OPCs remained in suspension. This step was repeated a second time, to yield highly pure OPC cultures. These cells were plated in an appropriate cell number onto PLL-coated cell culture dishes or glass coverslips with Super Sato. The day of OPC plating was defined as DIV-0 and cells were harvested for experiments at the subsequent days. After shaking off the OPCs, fresh DMEM (supplemented with 10% FCS, GlutaMAX, penicillin and streptomycin) was added to the remaining astrocytes and the cells were allowed to recover for 72 h. The astrocytes were then harvested for further experiments. The purity of these cells was determined separately by trypsinization, seeding onto PLL-coated cover- slips and immuno-staining after 48 h. The preparation of microglia was performed as described previously (Fitzner et al., 2011). In brief, glial mixed cultures were treated with microglia colony stimulating factor (MCSF) to enhance microglia proliferation. After 3 d, microglia were harvested by gentle shaking and seeded onto PLL-coated cell culture dishes with DMEM (supplemented with 10% FCS, GlutaMAX, penicillin and streptomycin). After another 3 d, cells were used for experiments. Cortical neuron cultures were prepared from embryonic mice at E16.5 as described with minor modifications (Sharma et al., 2015). Pregnant mice were killed by cervical dislocation and opened to reveal the embryos. The embryos were decapitated; the brains were exposed by a midline incision and transferred into HBSS. Meninges were stripped from the surface of the brain and hindbrain was discarded. Three brains were pooled, treated with 0.25% trypsin/EDTA for 10 min and washed with neuro- nal growth medium (MEM with B27-supplement, 0.6% glucose (wt/vol), 0.22% bicarbonate (wt/vol), pyruvate, GlutaMAX, penicillin and streptomycin). Cells were plated onto PLL-coated cell culture dishes with neuronal medium. After 16 h, cytosine arabinoside (AraC) was added in a final concentration of 4 μM. The addition was repeated the second day after plating. The third day, AraC was washed out and cells were cultivated in neuronal growth medium until day 5, 10 and 16, respectively.

METHOD DETAILS

Annotation of lipid classes and species

Glycerolipids are referred to as triacylglycerols (TAG) and diacylglycerols (DAG); glycerophospholipids and lyso-glycerophospholipids to phosphatidic acids (PA), phosphatidylinositols (PI), phosphatidylserines (PS), phosphatidylglycerols (PG), phosphatidylethanolamines (PE), phosphatidylcholines (PC), ether phosphatidylethanolamines (PE O-), ether phosphatidylcholines (PC O-), lyso-phosphatidic acids (LPA), lyso-phosphatidylinositols (LPI), lyso-phosphatidylcholines (LPC), and lyso-phosphatidylethanolamines (LPE); sphingolipids to ceramides (Cer) and sphingomyelins (SM); sterols to cholesterol (Chol) and cholesterylesters (CE) (Fahy et al., 2009). Lipid species are annotated according to their molecular composition as follows: [lipid class]-[sum of carbon atoms

in LCB and FAs]:[sum of double bonds in LCB and FAs];[sum of hydroxyl groups in LCB and FA] (e.g., SM 36:1;2 denotes sphingomyelin with a total length of its LCB and FA of 36; with 1 double bonds and 2 hydroxylations in total). For lipid subspecies, the individual acyl chain composition according to the same rule is given (e.g., 18:1;0_24:2;0), with the first entity denoting a sphingoid base (LCB) and the second a fatty acid (FA), in case of ceramides. Ceramides naming convention was adopted from Surma et al. (2015).

Lipid extraction for mass spectrometry lipidomics

Mass spectrometry-based lipid analysis was performed by Lipotype GmbH (Dresden, Germany) as described elsewhere (Sampaio et al., 2011). Lipids were extracted using a two-step chloroform/methanol procedure (Ejsing et al., 2009). Samples were spiked with internal lipid standard mixture containing: cardiolipin 16:1/15:0/15:0/15:0 (CL, 50 pmol), ceramide 18:1;2/17:0 (Cer, 30 pmol), diacylglycerol 17:0/17:0 (DAG, 100 pmol), hexosylceramide 18:1;2/12:0 (HexCer, 30 pmol), Sulfatide 18:1;2/12:0 (Sulf, 20 pmol), lyso-phosphatidate 17:0 (LPA, 30 pmol), lyso-phosphatidylcholine 12:0 (LPC, 50 pmol), lyso-phosphatidylethanolamine 17:1 (LPE, 30 pmol), lyso-phosphatidylglycerol 17:1 (LPG, 30 pmol), lyso-phosphatidylinositol 17:1 (LPI, 20 pmol), lyso-phosphatidylserine 17:1 (LPS, 30 pmol), phosphatidate 17:0/17:0 (PA, 50 pmol), phosphatidylcholine 17:0/17:0 (PC, 150 pmol), phosphatidylethanolamine 17:0/17:0 (PE, 75 pmol), phosphatidylglycerol 17:0/17:0 (PG, 50 pmol), phosphatidylinositol 16:0/16:0 (PI, 50 pmol), phosphatidylserine 17:0/17:0 (PS, 100 pmol), cholesterol ester 20:0 (CE, 100 pmol), sphingomyelin 18:1;2/12:0;0 (SM, 50 pmol), triacylglycerol 17:0/17:0/17:0 (TAG, 75 pmol) and cholesterol D6 (Chol, 300 pmol). After extraction, the organic phase was transferred to an infusion plate and dried in a speed vacuum concentrator. 1st step dry extract was re-suspended in 7.5 mM ammonium acetate in chloroform/methanol/propanol (1:2:4, V:V:V) and 2nd step dry extract in 33% ethanol solution of methylamine in chloroform/methanol (0.003:5:1; V:V:V). All liquid handling steps were performed using Hamilton Robotics STARlet robotic platform with the Anti Droplet Control feature for organic solvents pipetting.

MS data acquisition

Samples were analyzed by direct infusion on a QExactive mass spectrometer (Thermo Scientific) equipped with a TriVersa NanoMate ion source (Advion Biosciences). Samples were analyzed in both positive and negative ion modes with a resolution of $R_{m/z\ =\ 200}$ = 280000 for MS and $R_{m/z\ =\ 200}$ = 17500 for MSMS experiments, in a single acquisition. MSMS was triggered by an inclusion list encompassing corresponding MS mass ranges scanned in 1 Da increments (Surma et al., 2015). Both MS and MSMS data were combined to monitor CE, DAG and TAG ions as ammonium adducts; PC, PC O-, as acetate adducts; and CL, PA, PE, PE O-, PG, PI and PS as deprotonated anions. MS only was used to monitor LPA, LPE, LPE O-, LPI and LPS as deprotonated anions; Cer, HexCer, SM, LPC and LPC O- as acetate adducts and cholesterol as ammonium adduct of an acetylated derivative (Liebisch et al., 2006).

QUANTIFICATION AND STATISTICAL ANALYSIS

Data analysis and post-processing

Data were analyzed with in-house developed lipid identification software based on LipidXplorer (Herzog et al., 2011, 2012). Data post-processing and normalization were performed using an in-house developed data management system. Only lipid identifications with a signal-to-noise ratio > 5, and a signal intensity 5-fold higher than in corresponding blank samples were considered for further data analysis. Statistical analysis was performed with GraphPad Prism (GraphPad Software, Inc.). To perform multiple comparisons among two groups Sidak's multiple comparisons test was applied. To compare the interactions between different animal or cell cultures, two-way ANOVA followed by Tukey's post hoc test was used. A P value of < 0.05 was considered significant in all tests. All values are represented as mean ± SD.

Lipidome-related mouse brain proteome analysis

To analyze lipid-related protein expression across different cell types in the brain, the mouse brain proteome atlas resource was used (Sharma et al., 2015). This included the dataset on protein expression in cultured CNS cell types for individual replicates and developmental stages as well as the dataset on protein expression in brain regions. The Perseus software tool (versions 1.5.2.11 and 1.6.1.3) was used for bioinformatics analysis (Tyanova et al., 2016). In case of the cell type proteomes, protein LFQ intensities were log2-transformed and proteins filtered for experimental observations in at least two replicates of at least one cell entity (developmental stage-specific cell type).Missing values were imputed from a normal distribution based on default Perseus settings (distribution width 0.3, down-shift 1.8) and protein intensities were Z-scored across cell types. In case of brain region proteomes, the brain region means of log2-transformed LFQ-intensities were used and intensities were normalized by subtracting the the median across brain regions from protein intensities of individual regions. For both datasets, proteins were annotated with Gene Ontology (GO) annotations including GO biological process, GO cellular compartment, GO molecular function, KEGG annotations and with uniprot annotations including keywords, protein families and 'interacts with'. Moreover, proteins were annotated with metabolic pathway information from pathbank (http://pathbank.org) including generic pathways (1179 links of proteins to metabolic pathways) and more specific primary pathways (21709 links of proteins to primary metabolic pathways); files for murine protein annotation were kindly provided by the Wishart group maintaining Pathbank. Annotations were matched to proteins based on uniprot IDs. Proteins related to lipid dynamics/metabolism were manually shortlisted based on annotations in the categories Keywords, GO biological process, KEGG or pathbank primary metabolic pathway. In the cell type proteome dataset 580 lipid-related out of 8745 proteins were

selected while in the brain region proteome dataset 1027 lipid-related out of 8714 proteins were selected. For thehierarchical cluster analysis, lipid-related proteins were filtered and clustered according to Pearson correlation coefficients using the Perseus cluster tool. Clustering of cell type replicates was also based on Pearson correlation coefficients while clustering of brain regions was based on Euclidian distance. Enrichment of annotation terms in these clusters over the entire background dataset (8745 proteins for cell types, 8714 for brain regions) was calculated with Fisher's exact test. Annotations with a Benjamini-Hochberg-corrected p value above 0.15 in case of cell type data and a q-value above 0.05 in case of brain region data and annotations with an intersection size below three were excluded. To analyze specific annotation terms across cell types and brain regions, both datasets were transformed from protein abundance to annotation term abundance by taking the median abundance of all proteins associated with a given annotation term as the abundance of that term in each brain region or cell type replicate. The median of replicates was then taken as annotation abundance. Like proteins, annotation abundances were clustered based on Pearson correlation coefficients and cell types were as well clustered on Pearson correlation coefficients while brain regions were clustered based on Euclidian distance.